Monthly Notices
of the
ROYAL ASTRONOMICAL SOCIETY

Mon. Not. R. Astron. Soc. **413,** 1548–1568 (2011) doi:10.1111/j.1365-2966.2011.18238.x

The kinematic identification of a thick stellar disc in M31★†

M. L. M. Collins,[1]‡ S. C. Chapman,[1] R. A. Ibata,[2] M. J. Irwin,[1] R. M. Rich,[3] A. M. N. Ferguson,[4] G. F. Lewis,[5] N. Tanvir[6] and A. Koch[6]

[1]*Institute of Astronomy, University of Cambridge, Madingley Road, Cambridge CB3 0HA*
[2]*Observatoire de Strasbourg, 11 rue de l'Université, F-67000 Strasbourg, France*
[3]*Department of Physics and Astronomy, University of California, Los Angeles, CA 90095-1547, USA*
[4]*Institute for Astronomy, University of Edinburgh, Royal Observatory, Blackford Hill, Edinburgh EH9 3HJ*
[5]*Sydney Institute for Astronomy, School of Physics, A29, University of Sydney, NSW 2006, Australia*
[6]*Department of Physics & Astronomy, University of Leicester, University Road, Leicester LE1 7RH*

Accepted 2010 December 17. Received 2010 December 17; in original form 2010 October 25

ABSTRACT

We present the first characterization of a thick-disc component in the Andromeda galaxy (M31) using kinematic data from the DEIMOS instrument on Keck II. Using 21 fields in the south-west of the galaxy, we measure the lag of this component with respect to the thin disc, as well as the dispersion, metallicity and scalelength of the component. We find an average lag between the two components of $\langle \Delta v \rangle = 46.0 \pm 3.9\,\mathrm{km\,s^{-1}}$. The velocity dispersion of the thick disc is $\sigma_{\mathrm{thick}} = 50.8 \pm 1.9\,\mathrm{km\,s^{-1}}$, greater than the value of dispersion we determine for the thin disc, $\sigma_{\mathrm{thin}} = 35.7 \pm 1.0\,\mathrm{km\,s^{-1}}$. The thick disc is more metal poor than the thin disc, with $[\mathrm{Fe/H}]_{\mathrm{spec}} = -1.0 \pm 0.1$ compared with $[\mathrm{Fe/H}]_{\mathrm{spec}} = -0.7 \pm 0.05$ for the thin disc. We measure a radial scalelength of the thin and thick discs of $h_{\mathrm{r}} = 7.3 \pm 1.0$ and 8.0 ± 1.2 kpc, respectively. From this, we infer scaleheights for both discs of 1.1 ± 0.2 and 2.8 ± 0.6 kpc, both of which are approximately two to three times larger than those observed in the Milky Way. We estimate a mass range for the thick-disc component of $2.4 \times 10^{10} < M_{*,\mathrm{thick}} < 4.1 \times 10^{10}\,\mathrm{M}_{\odot}$. This value provides a useful constraint on possible formation mechanisms, as any proposed method for forming a thick disc must be able to heat (or deposit) at least this amount of material.

Key words: stars: kinematics and dynamics – galaxies: abundances – galaxies: evolution – Local Group – galaxies: spiral – galaxies: structure.

1 INTRODUCTION

Roughly 70 per cent of bright galaxies observed at redshift $z = 0$ possess stellar discs (e.g. Hammer et al. 2005; Choi, Park & Vogeley 2007; Park et al. 2007; Delgado-Serrano et al. 2010), including our own Galaxy and its two largest neighbours, M31 and M33. From this, we can infer that spiral morphologies are the dominant configuration for galaxies viewed at the present epoch. Under the formalism of hierarchical structure formation, galaxies are believed to evolve into their present forms via the accretion of, and mergers with, smaller systems. The effect of this process on the seemingly dynamically stable stellar discs we see in Milky Way (MW) type galaxies is still largely uncertain. The ability of these fragile objects to survive a 'major-merger' event (i.e. a merger with a system greater than one-third of the host's mass) is something that is still debated. Such major mergers are thought to be cosmologically common, with ∼70 per cent of all galaxies with a halo mass of $M \sim 10^{12}\,\mathrm{M}_{\odot}$ having experienced at least one major interaction within the past 8 Gyr (Stewart et al. 2008; Purcell, Kazantzidis & Bullock 2009). Thus, it has been argued that galaxies that possess thin stellar discs at $z = 0$ could not have experienced a major merger within the last 10 Gyr without the disc being destabilized (Toth & Ostriker 1992; Walker, Mihos & Hernquist 1996; Stewart et al. 2008; Purcell, Kazantzidis & Bullock 2009). This poses a significant challenge to our understanding of the formation of disc galaxies like the MW and M31. Recently, several authors have argued that these thin discs could survive such an event if the merging system is sufficiently gas rich (Robertson et al. 2006; Brook et al. 2007; Brooks et al. 2009;

★The data presented herein were obtained at the W. M. Keck Observatory, which is operated as a scientific partnership among the California Institute of Technology, the University of California and the National Aeronautics and Space Administration. The Observatory was made possible by the generous financial support of the W. M. Keck Foundation.
†Based on observations obtained with MegaCam, a joint project of CFHT and CEA/DAPNIA, at the Canada–France–Hawaii Telescope (CFHT) which is operated by the National Research Council (NRC) of Canada, the Institute National des Sciences de l'Univers of the Centre National de la Recherche Scientifique (CNRS) of France, and the University of Hawaii.
‡E-mail: mlmc2@ast.cam.ac.uk

Hopkins et al. 2009; Stewart et al. 2009), although the disc would still undergo heating, resulting in a thicker disc than that observed presently in the MW. In addition to the effect of major mergers on the structure of discs, galaxies viewed at the present epoch have undergone (and are still undergoing) many smaller 'minor' mergers which are not sufficiently massive to destroy thin stellar discs, but are thought to kinematically heat them, causing them to flare outwards and create a second, thick-disc component (Quinn, Hernquist & Fullagar 1993; Robin et al. 1996; Walker et al. 1996; Velazquez & White 1999; Chen et al. 2001; Sales et al. 2009; Villalobos & Helmi 2009; Purcell, Bullock & Kazantzidis 2010). Other physical processes are also thought to heat up and thicken the thin disc, including the accretion of a satellite on a radial orbit about its host (Abadi et al. 2003; Read et al. 2008), internal heating within the disc from massive star clusters, interactions with spiral arms, etc. (Villumsen 1985; Carlberg 1987; Hänninen & Flynn 2002; Sellwood & Binney 2002; Benson et al. 2004; Hayashi & Chiba 2006; Kazantzidis, Zentner & Kravtsov 2006; Roškar et al. 2008; Schönrich & Binney 2009a; Loebman et al. 2010). Thick discs may also have formed thick, with significant star formation occurring above the mid-plane of the galaxy or with large initial velocity dispersions (Kroupa 2002; Brook et al. 2004). In recent work by Roškar et al. (2010), they suggest that *in situ* formation could also occur if the stellar disc is misaligned with the hot, gaseous halo. This misalignment results in a significant warping of the outer disc, and subsequent star formation within this warp results in a low-metallicity thick disc. Finally, it is also possible that a number of these mechanisms will act in conjunction. In particular, it has been suggested by a number of authors that secular growth from internal heating may be significantly enhanced by minor-merger events via swing amplification (e.g. Sellwood, Nelson & Tremaine 1998; Dubinski et al. 2008), as these processes often occur simultaneously. As such, it makes little sense to treat these two scenarios as separate processes.

With so many potential mechanisms capable of producing thickened stellar discs, just how common are thick discs in spiral galaxies at the present epoch? Dalcanton & Bernstein (2002) claim that thick-disc formation is a universal feature of disc formation and as such should be observed in all spiral galaxies. Whether such discs are formed predominantly via one mechanism, or a mixture of them, is still uncertain and disentangling the various formation scenarios from one another in present data sets has proven difficult.

In the MW, the existence of a thick disc has long been known and was first identified by Gilmore & Reid (1983). Subsequent spectroscopic studies of this component have shown it to be kinematically distinct from the thin stellar disc, with the thick disc lagging behind the thin disc by $\sim$50 km s^{-1} (Carollo et al. 2010) and having a larger velocity dispersion than the thin disc. This thick-disc component also seems to be composed of older, more metal deficient stars (e.g. Chiba & Beers 2000; Wyse et al. 2006). However, the observed properties of the thick disc, such as scaleheight, scalelength and velocity dispersion, tend to vary depending on the survey sample and tracer population used (Ivezić et al. 2008; Jurić et al. 2008; Carollo et al. 2010; de Jong et al. 2010). As such, the origin of the MW thick disc is still a subject of great debate in the literature. Thick discs have also been observed in a number of edge-on spiral galaxies (e.g. Burstein 1979; Tsikoudi 1979; van der Kruit 1984; Shaw & Gilmore 1989; van Dokkum et al. 1994; Dalcanton & Bernstein 2002; Elmegreen & Elmegreen 2006; Yoachim & Dalcanton 2006, hereinafter YD06; Yoachim & Dalcanton 2008a,b), and spectroscopic observations of these objects also show the thick discs to be composed of older stars than their corresponding thin discs. However, as these galaxies are all located at distances greater than $\sim$10 Mpc from the MW, one cannot obtain spectra for individual stars and must instead rely on the integrated spectral properties of red giant branch (RGB) stars. Obtaining spectra with a high enough signal-to-noise ratio (S/N) to discern velocity dispersion profiles and reliable metallicities is also challenging, making it impossible to distinguish between the various formation mechanisms for these structures.

If thick stellar discs are universal amongst spiral galaxies and are formed by mergers with, or accretions of, satellites, one might expect to see such a structure in M31. This neighbouring galaxy is considered to be a 'typical' spiral galaxy when compared with other local external disc galaxies (Hammer et al. 2007). It is thought to have had an active merger history, and a recent panoramic photometric survey by the Pan-Andromeda Archaeological Survey collaboration (McConnachie et al. 2009) has shown the halo of this galaxy to be littered with tidal streams from interactions with infalling satellites. These include the Giant Southern Stream (GSS, Ibata et al. 2001; Gilbert et al. 2009) and streams A, B, C, D and E (Ibata et al. 2007; Chapman et al. 2008; McConnachie et al. 2009). The outer disc of M31 is very perturbed (Ferguson et al. 2002; Richardson et al. 2008), suggestive of some tidal interaction. M31 is also host to 25 known dSph and four dE satellites, at least two of which (NGC 205 and M32) show evidence for significant tidal interaction (Choi, Guhathakurta & Johnston 2002; McConnachie et al. 2004a; Geha et al. 2006; Howley et al. 2008). Therefore, the possibility of numerous interactions between the disc of M31 and its satellite population seems highly likely. McConnachie et al. (2009) also present evidence for a recent interaction between M31 and its neighbouring spiral galaxy, M33, which could have significantly distorted and heated the M31 disc, giving rise to a thick-disc component or substantial substructure in the outer disc. Other groups have postulated links between the formation of bulges and thick discs in spiral galaxies (Hopkins et al. 2008; Meléndez et al. 2008; Bournaud, Elmegreen & Martig 2009; Bensby et al. 2010), and as M31 is known to have a reasonably massive bulge (Saglia et al. 2010), it is an interesting candidate for hosting a thick disc. Despite its high inclination to us along the line of sight (77°, Walterbos & Kennicutt 1988), M31 is not seen sufficiently edge-on to allow us to look for such a population using photometry. Therefore, to look for evidence of a thick disc in M31, we must search for it via its kinematic signature, using spectroscopy. Given its proximity to us (785 kpc, McConnachie et al. 2005), M31 is an ideal target for spectroscopic observations as we are able to resolve and obtain reliable velocities for individual RGB stars, and it has an advantage over our own Galaxy as we are afforded a panoramic view, whereas in the MW we are hampered along various lines of sights by confusion from the disc and the bulge.

Since 2002 our group has been conducting a systematic spectroscopic survey of M31, including the disc, halo and regions of the substructure using the DEIMOS instrument mounted on the Naysmyth focus of Keck II (Ibata et al. 2005, hereafter I05; Chapman et al. 2006, 2007, 2008; Collins et al. 2009, 2010). The data from this survey give us an ideal opportunity to identify a thick disc if present. In fact, in their study of M31's extended disc using this same data set, I05 identified a population lagging behind the thin disc, which they excluded from their study, termed a 'thick-disc-like' population, and Chapman et al. (2006) briefly examined this component as a function of the radius but were unable to comment on its global properties. In this work, we discuss the results from an in-depth study of this population, analysing its kinematics and chemistry, comparing them to M31's thin and extended

discs, the thin and thick discs in the MW, and those seen in other galaxies, and comment on possible formation scenarios for this component.

This paper is set out as follows. In Section 2, we discuss the known structure of M31. Section 3 focuses on our spectroscopic survey of M31 and discusses field selection and analysis techniques. We present our results in Section 4 and discuss their implications in Section 5. We conclude our findings in Section 6.

2 THE BULGE, DISCS AND HALO OF M31

The first recorded observation of M31 was made in AD 964 in the 'Book of constellations and fixed stars' written by the Persian astronomer, Abd al-Rahman al-Sufi, who described it as 'a small cloud' in the night sky. In the centuries that have passed since, M31 has been a popular target for astronomers, and much has been learned about its structure. M31 is a spiral galaxy of SA(s)b type, with a significant bulge, a classical thin stellar disc, a vast extended stellar disc and a metal-poor halo. In this section, we outline the properties of each of these components.

First, we discuss the bulge component. Numerous studies have shown that M31 possesses a classical bulge, with a Sérsic index of $\sim$2 and an effective radius of 1.93 kpc (Kormendy & Bender 1999; Seigar, Barth & Bullock 2008). It is largely supported by random motions, although recent work by Saglia et al. (2010) has found evidence for rotation in the innermost regions. Saglia et al. also find the bulge to be dominated by an old stellar population (age $\gtrsim$ 12 Gyr) of roughly solar metallicity, with a large velocity dispersion of 166–170 km s^{-1}. This component is dominant out to about 8 arcmin ($\sim$2 kpc), at which point the disc begins to dominate the surface brightness profile of the galaxy (Saglia et al. 2010); however, according to Merrett et al. (2006), the bulge can be traced out as far as 10 effective radii, equivalent to $\sim$15 kpc, meaning that some of our innermost disc fields may be subjected to minor contamination from this component.

Studies of the thin stellar disc of M31 have been performed by a number of authors (e.g. Walterbos & Kennicutt 1988; Ferguson & Johnson 2001; I05; Ibata et al. 2007; McConnachie et al. 2009) and have challenged our previous notions of the structure of classical discs. With a scalelength of 5.9 kpc (Walterbos & Kennicutt 1988, corrected for an assumed distance to M31 of 785 kpc; Merrett et al. 2006), it is more extensive than that of our Galaxy and also appears to be forming stars at a lower rate (Walterbos & Braun 1994), and while it is a characteristic feature of the surface brightness profiles of stellar discs to steeply decline at 3–4 scalelengths (van der Kruit & Searle 1981; Pohlen, Dettmar & Lütticke 2000), which corresponds to 18–24 kpc in M31, a spectroscopic study by Ibata et al. (2005) uncovered a vast, extended disc component that can be traced out to distances of $\sim$40 kpc ($\sim$8 scalelengths) from the centre of the galaxy that has an exponential surface density profile that is very similar to the inner disc. While this structure is rather clumpy, on average, it appears to follow on smoothly from the classical inner disc, although perhaps with a slightly larger scalelength of 6.6 $\pm$ 0.6 kpc and with a slight lag behind circular velocities at large radii ($\langle \Delta v \rangle = 20$ km s^{-1}, I05). It is dynamically cold, with a velocity dispersion ranging from 20 to 40 km s^{-1}, leading I05 to conclude that it is likely not a thickened disc. Whether this extended component is truly separate from the classical thin disc, or merely an extension of it that shows some evidence of heating and warping at larger radii where the disc is more sensitive to perturbations from mergers and interactions, is unclear. Owing to the similarity of the thin and extended discs, we will refer to them both as the 'thin disc' throughout this paper. Where we wish to make a distinction between the two, we shall use the terminologies 'classical' and 'extended' discs.

The presence of a smooth, pressure-supported metal-poor halo in M31 eluded detection until very recently. In 2006, two groups (Chapman et al. 2006; Kalirai et al. 2006) independently identified such a component using the DEIMOS instrument on the Keck II telescope. Centred on the systemic velocity of M31, with a central velocity dispersion of 152 km s^{-1}, and showing no strong evidence of rotation, both groups found this component to be metal poor with an average metallicity of [Fe/H] $= -1.4 \pm 0.2$ (Chapman et al. 2006). Kalirai et al. (2006) were able to trace this component out as far as 165 kpc from the centre of the galaxy, although there is an inevitable confusion with the halo of M33 at these large distances (Ibata et al. 2007; Koch et al. 2008; McConnachie et al. 2009).

The halo of M31 is also a known host to a number of kinematic substructures, such as the GSS, the tangential streams that cross the south-east minor-axis, the western shelf and a wealth of substructure in the north-east (NE) of the galaxy that is thought to be linked to the GSS. In the following analysis, we will carefully consider the kinematics of all these components to ensure any thick-disc sample that we define is free from contamination by any of these sources. We shall discuss this in greater detail in Section 3.

3 OBSERVATIONS AND FIELD SELECTION

A detailed description of the observational methodology and target selection employed in the survey is given in I05, which we briefly summarize here. Using colour–magnitude diagrams (CMDs) from both the Canada–France–Hawaii (CFHT) and Isaac Newton (INT) telescopes (Ferguson et al. 2002; Ibata et al. 2007; McConnachie et al. 2009), we selected targets for observation by prioritizing RGB stars in M31 with $20.5 \leq i \leq 21.2$ and colours $1.0 \leq (V - i)_0 \leq 4.0$ (priority A), and then filling the remainder of the masks with stars with $I \leq 22.0$ that are unsaturated (priority B), where the V and I colours are transformed from their native g and i colours using the relations described in McConnachie et al. (2004b) and Ibata et al. (2007). We used a combination of standard DEIMOS multislit mode for low-density fields, such as the halo, and our own minislitlet approach which allowed us to target >600 stars per mask in more crowded regions, such as the disc. Our observational setup covers the range of the calcium triplet (Ca II) lines at 8498, 8542 and 8662 Å, a prominent absorption feature that can be used both to measure radial velocities and as a metallicity indicator. To obtain velocities, we cross-correlate all observed stars with a template Ca II spectrum. We estimate the errors on our velocities by following the procedures of Simon & Geha (2007) and Kalirai et al. (2010). First, we make an estimate of our velocity uncertainties for each observed star using a Monte Carlo (MC) method, whereby noise is randomly added to each pixel in the spectrum, assuming a Poisson distribution for the noise, and the velocity is recalculated using the same cross-correlation technique as described above. This procedure is repeated 1000 times and then the error is calculated to be the square root of the variance of the resulting mean velocity. We combine this error with a systematic error, ϵ, which contains information on any errors we may not have accounted for (e.g. wavelength calibration error, misalignment of the mask, etc.). For the fields observed with the 600 lines mm^{-1} grating, we evaluate this error directly by using repeat measurements in fields 231Dis and 232Dis, a total of 332 stars. We

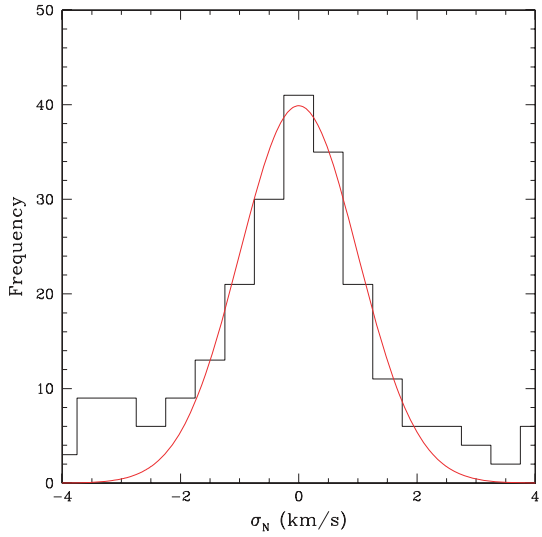

Figure 1. A histogram showing the normalized error distribution for repeat measurements of the same stars in two of our fields that were observed with the 600 lines mm^{-1} grating. The normalized error, σ_N, incorporates the velocity differences between the repeat measurements (v_1 and v_2) and the MC uncertainties calculated for each observation (σ_1 and σ_2). In order to reproduce a unit Gaussian distribution for our uncertainties, we also include an additional error term, ϵ, which accounts for any systematic uncertainties we have not included. We find $\epsilon = 5.6$ km s^{-1} for this setup. For fields using the 1200 lines mm^{-1} setup, we use the Simon & Geha (2007) value of $\epsilon = 2.2$ km s^{-1}.

define the normalized error, σ_N, as

$$\sigma_N = \frac{v_1 - v_2}{(\sigma_1^2 + \sigma_2^2 + 2\epsilon^2)^{1/2}}, \quad (1)$$

where v_1 and v_2, and σ_1 and σ_2 are the velocities and errors of each measurement pair, and ϵ is the additional random error required in order to reproduce a unit Gaussian distribution with our data (shown in Fig. 1) This gives us a systematic error for this setup of $\epsilon = 5.6$ km s^{-1}, slightly lower than the value of $\epsilon = 6.2$ km s^{-1} derived by Collins et al. (2010) for the same setup, though we note that their measurement was based on repeat observations of 47 stars, compared with our much larger data set of 332 stars. The typical uncertainties for these measurements above a threshold of S/N = 3 are 5–10 km s^{-1}.

The Ca II features also provide us with a method for measuring the spectroscopic metallicity of our observed sample. Following the procedure of Rutledge, Hesser & Stetson (1997) and Battaglia et al. (2008), we fit Gaussian functions to the three Ca II peaks to estimate their equivalent widths (EWs), and calculate [Fe/H] using equation (1)

$$[\mathrm{Fe/H}] = -2.66 + 0.42[\Sigma\mathrm{Ca} + 0.64(V_{\mathrm{RGB}} - V_{\mathrm{HB}})], \quad (2)$$

where $\Sigma\mathrm{Ca} = 0.5\,\mathrm{EW}_{8498} + \mathrm{EW}_{8542} + 0.6\,\mathrm{EW}_{8662}$, V_{RGB} is the magnitude (or, if using a composite spectrum, the average magnitude) of the RGB star and V_{HB} is the mean V magnitude of the horizontal branch (HB). Using $V_{\mathrm{HB}} - V_{\mathrm{RGB}}$ removes any strong dependence on the distance or reddening in our calculated value of [Fe/H] and gives us the Ca II line strength at the level of the HB. For M31, we set this value to be 25.17 (Holland, Fahlman & Richer 1996). We note that this assumed value is sensitive to age and metallicity effects (see Chen, Zhao & Zhao 2009 for a discussion); however, owing to the large distance of M31, small differences in this value within the disc of M31 will have a negligible effect on metallicity calculations. For individual stars, these measurements carry large errors ($\gtrsim$0.4 dex), but the errors are significantly reduced when stacking the spectra into a composite in order to measure an average metallicity for a given population.

3.1 Field selection and sample definition

In order to detect a thick-disc component in M31 kinematically, we need to measure the velocities of stars within our sample relative to some model for the velocity of stars within the thin disc of the galaxy. If a thick disc is present, we should observe a population that lags behind the thin disc in terms of its rotational velocity. The component is also expected to have a larger velocity dispersion than the thin disc. This is observed in the MW, where the thick disc lags the thin one by 20–50 km s^{-1} (Chiba & Beers 2000; Soubiran, Bienaymé & Siebert 2003) and has an average rotational velocity dispersion of $\sigma_{V_\phi} = 57$ km s^{-1} (Carollo et al. 2010). For the purposes of this work, we shall use an updated version to the disc model of I05. In this model, we assume circular orbits for all stars about the centre of M31 and interpolate their velocities from the H I rotation curve of Chemin et al. (2009), which is shown in Fig. 2 as the solid black points. This rotation curve differs from that adopted by I05, particularly in the outermost regions. They used a compilation of CO data from Klypin, Zhao & Somerville (2002) and H I data from Brinks & Burton (1984), which we also show in Fig. 2 as red triangles. We also show the H I rotation curve derived by Corbelli et al. (2010) from a WRST survey (Braun et al. 2009) as blue squares. Using either of these rotation curves as opposed to that of Chemin et al. leads to differences in our interpolated velocities of the order of a few to 20 km s^{-1}; however, there is a negligible effect on the dispersions within particular populations and so the adoption of any of these curves would give us consistent results when analysing the global properties of the stellar discs in this work. We assume an inclination for M31 of 77° (Walterbos & Kennicutt 1988) and adopt parameters for the thickness of the disc identical to those used in I05, with a constant thickness for the disc of 350 pc (which is roughly the thickness of the MW disc, Ivezić et al. 2008) out to

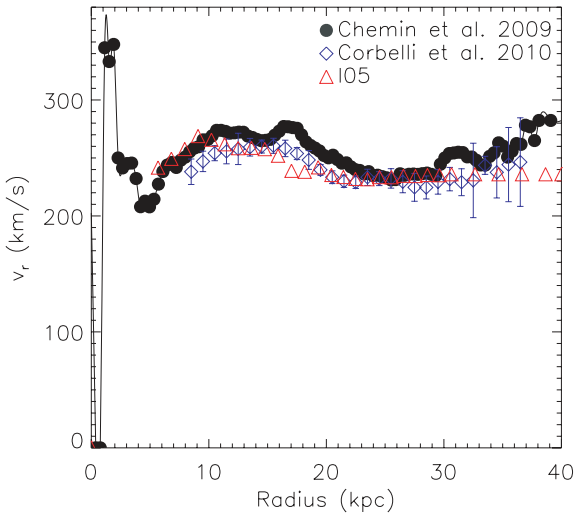

Figure 2. Here we show a number of H I rotation curves for M31. Throughout this work, we use results based on the Chemin, Carignan & Foster (2009) work, shown as filled black circles. We also show rotation curves from Corbelli et al. (2010) and I05, which differ slightly from the Chemin et al. (2009) curve in the outermost regions. We find that using these curves versus the Chemin et al. (2009) results does not affect our results.

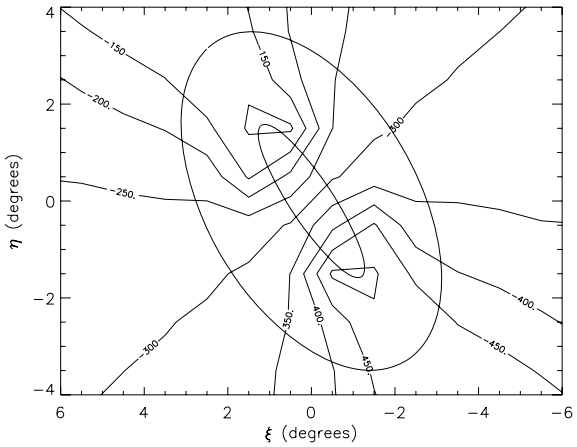

Figure 3. A contour map of the expected velocities of stars in circular orbits in the disc of M31. This was constructed using our simple model as discussed in Section 3.

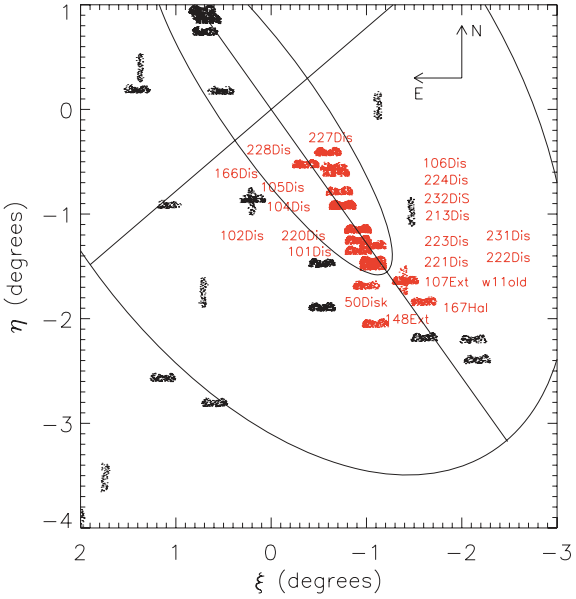

Figure 4. Map showing the location of fields within our M31 survey. Fields selected for study in this work are labelled and highlighted in red. The outer ellipse shows a segment of a 55-kpc-radius ellipse flattened to $c/a = 0.6$, and the major-axis and minor-axis are indicated with straight lines out to this ellipse. The inner ellipse corresponds to a disc of radius 2° (27 kpc), with the same inclination as the main M31 disc.

16 kpc, at which point we assume the stellar disc begins to flare with a scaleheight that increases linearly with the radius. We set a maximum scaleheight of 1.69 kpc at a radius of 30.5 kpc, beyond which we assume that the disc has constant thickness. We then integrate along the line of sight through this flaring exponential disc and project the velocities of objects on circular orbits about M31 on to the line of sight. This produces an average velocity map for the disc of M31, which we display in Fig. 3.

Once our disc model has been constructed, we need to select a sample of fields from our DEIMOS survey that will provide the most reliable kinematic comparison with respect to the velocity of the disc. As the disc of M31 is not infinitesimally thin, but possesses some unknown scaleheight, any line of sight taken through the galaxy traverses a significant depth. Given the inclination of M31, some lines of sight will traverse larger depths than others, which could have the effect of smearing out the velocities of objects with respect to the disc model. This is illustrated in fig. 8 of I05. They find that objects along the major-axis of M31 are less susceptible to this effect than those that are located off the major-axis, and therefore we limit our initial study to fields along the major-axis.

A further complication in field selection arises from MW contamination. Our colour-selection criteria mean that we inevitably observe Galactic K dwarf stars within our sample, as these lie coincident with M31 RGB stars in the CFHT and INT CMDs. Eliminating these stars from our sample is straightforward in the south-west (SW) region of M31, as the disc of Andromeda and the halo of the MW occupy distinct positions in the heliocentric velocity space. Assuming the Besancon model is a good description of the foreground populations in the direction of M31, it can be shown that the Galactic population peaks at $v_{\rm hel} = -61\,{\rm km\,s^{-1}}$, and the contribution of MW K dwarfs to our sample at $v_{\rm hel} \leq -100\,{\rm km\,s^{-1}}$ is very low (Robin et al. 2004; I05). Given that the average rotational velocity in the SW of M31 is less than $-300\,{\rm km\,s^{-1}}$ (I05), we are able to cleanly separate M31 stars from MW field stars. However, in the NE of M31, the average heliocentric velocity of the M31 disc typically ranges between -100 to $-200\,{\rm km\,s^{-1}}$, resulting in a significant overlap between Galactic and M31 populations, making it difficult to distinguish between the two. While it is possible to remove some of this contamination by examining the strength of the sodium doublet (Na I), located at a rest wavelength of ∼8190 Å, this is not a perfect discriminator. One can also eliminate some foreground contamination via a comparison of photometric and spectroscopic metallicities (Gilbert et al. 2006), but given the uncertainties on the individual spectroscopic [Fe/H] of our observed stars (discussed above), we still retain a significant population of contaminants within our sample. There is also contamination in the NE from the M31 substructure (I05; Chapman et al. 2006; Richardson et al. 2008) which can be difficult to separate from the M31 disc in the NE. For these reasons, we limit our initial study to the SW major-axis. We hope to analyse the NE population in a future paper. These criteria leave us with a sample of 21 fields along the SW major-axis, highlighted in red in Fig. 4. The positions and properties of these fields can be found in Table 1. Two of these fields (231Dis and 232Dis) were observed as part of our ultradeep M31 disc survey (Chapman et al., in preparation) and were integrated for 4.5 h with the 600 lines mm^{-1} grating, which allowed us to make more robust measurements of individual stellar metallicities than for our other fields.

To isolate a potential thick-disc population in our sample of 21 fields, we must first define a statistical measure of what constitutes a lagging population with respect to the thin and extended discs. We must also ensure that our definition is able to distinguish between this population and that of the metal-poor M31 halo which, as it is a non-rotating component (Chapman et al. 2006; Kalirai et al. 2006), also lags behind the disc. In Fig. 5, we display two histograms, one with the heliocentric velocities ($v_{\rm hel}$) of the stars in our 21 fields and the other with their velocities with respect to the disc ($v_{\rm lag}$), and we highlight the regions we expect each of these components to inhabit, along with where we expect to see contamination from halo K dwarfs in the MW.

We do this using two separate methods. The first is to fit Gaussians to both a disc component, located on or around $v_{\rm lag} = 0\,{\rm km\,s^{-1}}$, and a broad halo component centred on or around $v_{\rm lag} = -300\,{\rm km\,s^{-1}}$. We then define a thick-disc population to encapsulate anything that lags the thin disc by $>2\sigma$ of the thin-disc peak value and we implement a lower cut on this population by requiring that the contribution

Table 1. Properties of fields analysed in this work.

Field	Date observed	α_{J2000} (hh:mm:ss)	δ_{J2000} (°:′:″)	Grating (lines mm^{-1})	PA (°)	Exposure time (s)	Number of targets	R_{proj} (kpc)
228Dis	23/09/2006	00:40:50.56	40:43:54.0	1200	90	3600	301	9.8
227Dis	23/09/2006	00:39:37.40	40:50:42.0	1200	90	3600	312	15.6
166Dis	03/10/2005	00:39:17.89	40:42:18.0	1200	90	3600	209	15.8
106Dis	30/08/2005	00:39:10.00	40:39:00.0	1200	90	3600	257	16.1
105Dis	30/08/2005	00:39:00.00	40:28:12.0	1200	90	3600	271	16.2
224Dis	25/09/2006	00:38:50.00	40:20:30.0	1200	90	3600	265	16.6
232Dis	05/10/2006	00:38:50.00	40:20:00.0	600	90	16 200	184	16.6
104Dis	30/08/2005	00:38:50.00	40:20:00.0	1200	90	3600	271	16.7
220Dis	22/09/2006	00:38:00.00	40:06:12.0	1200	90	3600	322	20.3
213Dis	22/09/2006	00:38:11.60	40:06:12.0	1200	90	3600	155	20.5
102Dis	30/08/2005	00:38:00.00	40:00:00.0	1200	90	3600	268	21.5
231Dis	05/10/2006	00:38:00.00	40:00:00.0	600	90	16 200	185	21.6
223Dis	25/09/2006	00:37:12.00	39:57:00.0	1200	90	3600	304	23.2
101Dis	30/08/2005	00:38:00.00	39:54:00.0	1200	90	3600	275	23.5
222Dis	22/09/2006	00:37:12.49	39:48:06.0	1200	90	3600	298	24.9
221Dis	22/09/2006	00:37:11.97	39:45:00.0	1200	90	3600	303	25.8
50Disk	16/09/2004	00:37:35.29	39:33:55.0	1200	90	3600	216	30.1
107Ext	30/08/2005	00:35:28.00	39:36:19.1	1200	90	3600	265	31.0
w11old	30/09/2002	00:35:27.02	39:37:15.3	1200	90	3600	95	31.0
167Hal	03/10/2005	00:34:30.24	39:23:58.7	1200	90	3600	205	34.2
148Ext	04/10/2005	00:37:07.23	39:12:00.0	1200	90	3600	211	39.6

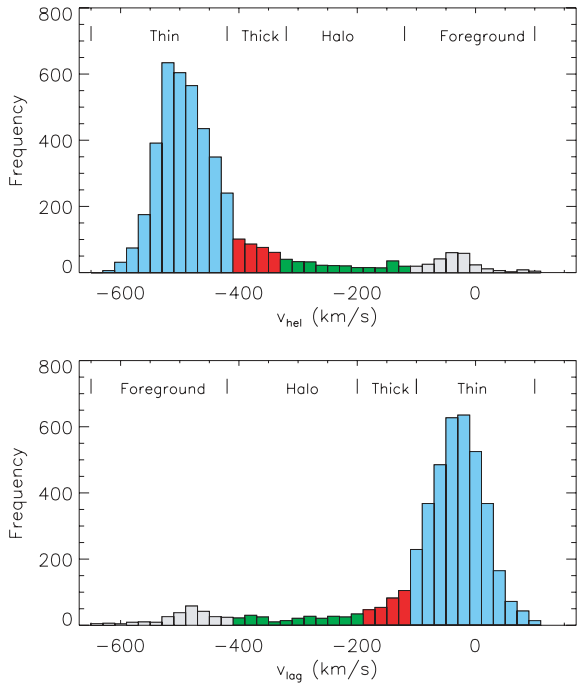

Figure 5. Histograms for both heliocentric (top panel) and disc lag (bottom panel) velocities of all stars within our sample of 21 fields. Regions expected to be inhabited by thin-disc (light blue), thick-disc (red), halo (green) and MW foreground (grey) are highlighted.

from the halo would be <1 star per velocity bin (20 km s^{-1}), thus minimizing the contamination. In fields where there is no obvious halo component to fit to, we use a Gaussian centred on −300 km s^{-1} with a dispersion of 90 km s^{-1} (Chapman et al. 2006) and normalize it with respect to the thin disc by assuming that the halo contributes ∼10 per cent to the total number of stars within the field (a conservative estimate, given that the stellar halo contributes ≪10 per cent to the total stellar light in disc galaxies). The second method is to fit multiple component Gaussians to each of the fields. We apply a Gaussian Mixture Modelling (GMM) technique, which allows the number of Gaussians to vary freely between one to seven components. To discern which model best fits the data, we apply a likelihood ratio test (LRT) to the resulting probabilities of the fits. The use of the LRT in astronomy was popularized by Cash (1979) and is often used in the literature to determine whether the properties of an observed stellar population can be well described by single versus multiple Gaussian components (e.g. Ashman, Bird & Zepf 1994; Carollo et al. 2010). The LRT compares the likelihoods of nested models (in our case, a mixture of Gaussian components) to determine whether applying a model with additional parameters produces a significantly better fit than a simpler model. This is done by calculating the LRT statistic, $-2\ln(\mathcal{L}_1/\mathcal{L}_2)$, where $\mathcal{L}_1$ and $\mathcal{L}_2$ represent the likelihoods of the simple and complex models, respectively, and comparing it with a χ^2 distribution with degrees of freedom equal to the difference between the number of parameters in the two models (three in our case). For a model with additional parameters to be accepted as a statistically better fit, this ratio must be greater than 7.82 which corresponds to a P value of <0.05. In general, this technique converges on fits with three components (a thin disc, a halo and a thick population), though there are a few exceptions. We shall discuss these fits in greater detail in the following section. Where this technique converges on fits that identify a lagging component that is distinct from both the thin disc and halo, we define a sample of highly probable thick-disc stars by applying a standard Bayesian classification scheme to assign each star a probability of being a member of the thin-disc, P(thin), thick-disc, P(thick), or halo, P(halo), population based on their velocity, and the properties of the Gaussian fits to each population on a field-by-field basis. We define a star as being a highly probable member of the thick disc if $P(\text{thick}) \geq 0.997$. The results of both these techniques can be seen in Fig. 6. The velocity cuts for stars selected using our 2σ technique are shown as dashed lines and the range of velocities selected using the Bayesian classification technique are marked with solid lines. It can be seen that both techniques isolate a very similar population. In Fig. 7, we plot a CMD showing the

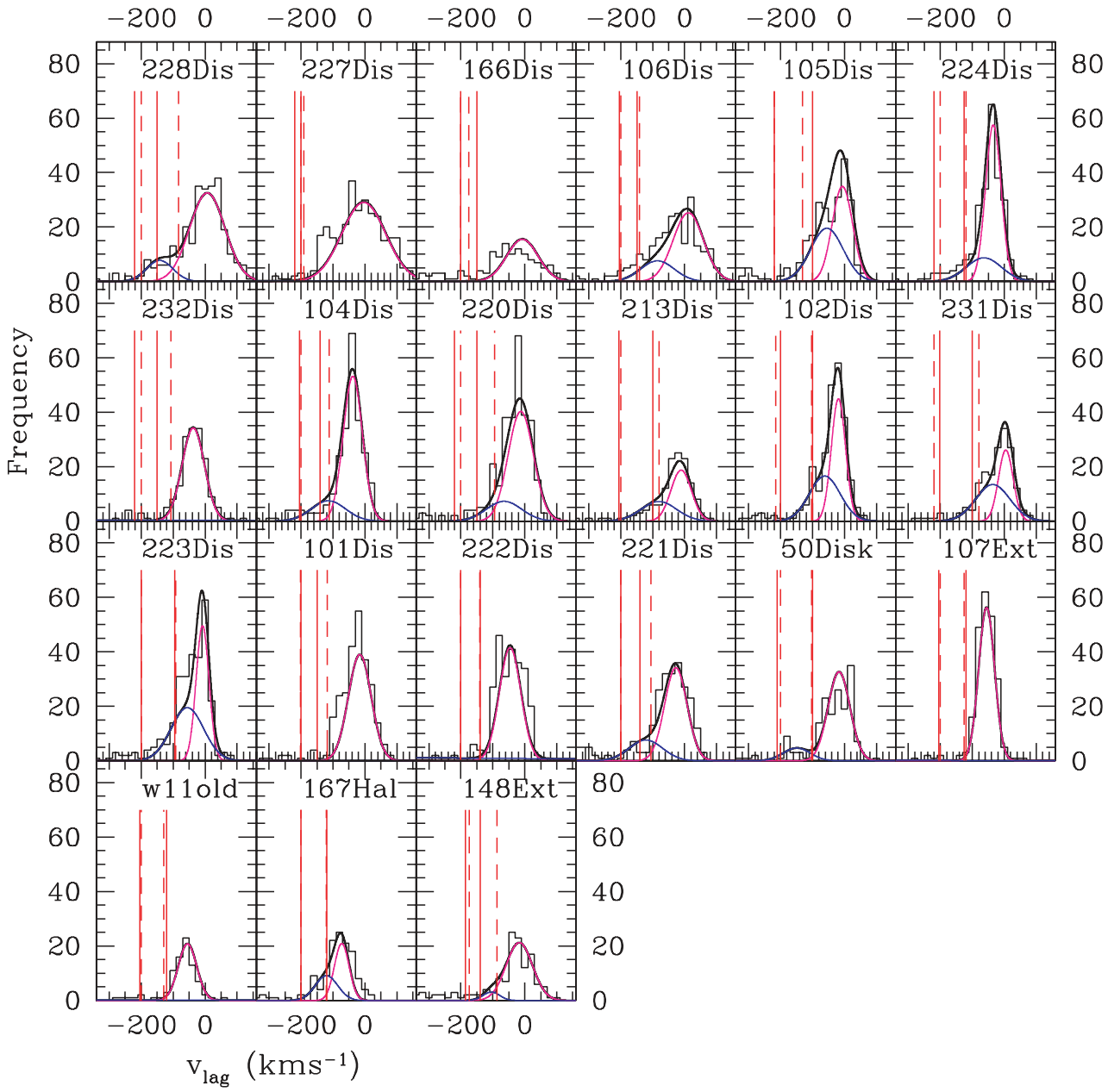

Figure 6. Our initial sample of fields, selected for their position along the SW major-axis as described in the text, are shown in order of increasing (projected) radius. Gaussian fits indicating the thin and (where applicable) thick discs are shown as magenta and blue curves, respectively. Our selection criteria are overlaid, with the dashed lines representing our 2σ cuts and the solid lines representing our Gaussian cuts both of which sample roughly the same region of velocity space.

$V - I$ colours of the thin (blue points) and thick (magenta points) populations, and we overlay Dartmouth isochrones (Dotter et al. 2008) of $[\alpha/\mathrm{Fe}] = +0.2$ and an age of 8 Gyr (in line with the estimated range of ages for the thin disc of 4–8 Gyr, Brown et al. 2006) with metallicities ranging from $[\mathrm{Fe/H}] = -0.4$ to -1.5. Both thin- and thick-disc populations inhabit roughly the same region in this CMD, which we shall discuss in more detail in Section 4.3.

Finally, we note that in both selection methods, we expect some cross-contamination between the thin- and thick-disc components, as the two populations significantly overlap. However, we assume this contamination will be lower in our cuts based on the Gaussian fits, as these are more conservative. Therefore, we use these cuts predominantly in this paper when referring to clean thin- and thick-disc samples. We have also assumed both components have symmetric, Gaussian distributions in velocity, which may not be the case, and this could cause further contamination if the populations are skewed. We also expect some contamination from the halo; however, given that the disc is the dominant population in all our fields, we expect this contamination to be negligible in comparison to the cross-contamination between the discs.

3.2 Testing the statistical significance of our sample

Before we analyse our sample, we test the significance of our thick population to ensure it is not merely consistent with noise above a thin-disc population plus smooth halo component. To do this, we

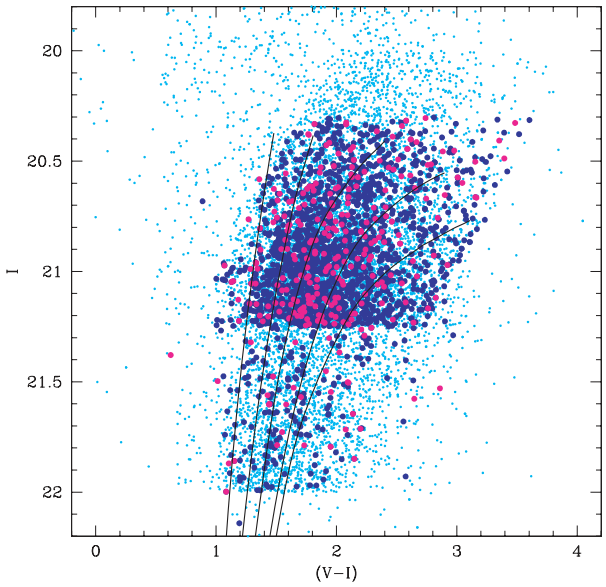

Figure 7. CMD for our thin (blue points) and thick (magenta points) populations in standard Landolt V and I colours. Dartmouth isochrones with $[\alpha/\mathrm{Fe}] = +0.2$ and an age of 8 Gyr are overlaid with metallicities, from the left-hand to right-hand side, of [Fe/H] $= -1.5$, -1.0, -0.5 and -0.4. The colours of the remaining stars in our DEIMOS survey are also plotted in light blue.

fit a single Gaussian to the disc and halo components, as described above and then calculate the deviation of the data from the fit for all velocities greater than the peak disc velocity (i.e. the right-hand side of the disc fit), normalizing it to the expected contribution from the Gaussian in this region. We then define the noise to be 1.5 times the median absolute deviation of this sample. We repeat this exercise for all velocities less than the thin-disc peak and greater than $-200\,\mathrm{km\,s^{-1}}$ in the lag frame, in this case comparing to the expected contribution from both thin-disc and halo fits. This allows us to work out the significance of our thick-disc population, σ_{conf}. In all cases where the GMM identified a thick-disc component, we find that our excess above the thin disc plus halo model has a significance of $>3\sigma$ (see Table 2). For the fields where the GMM converged on a two-Gaussian fit (232Dis, 222Dis, 107Ext and w11old), we find $\sigma_{\mathrm{conf}} < 3\sigma$. We also identify an additional three fields (101Dis, 166Dis and 227Dis), where $\sigma_{\mathrm{conf}} < 3\sigma$. Two of these fields are located at radii of $\sim$15 kpc, where there may be residual contamination from the bulge component. This may also explain the large dispersions (of the order of $50\,\mathrm{km\,s^{-1}}$) seen in our innermost fields. Excluding these, we are left with 14 of our 21 (2/3) fields where we confidently detect a thick component. We shall focus on these fields in the remainder of our analysis, but we shall discuss the significance of the non-detections in Section 5.

Table 3. Average properties of the thin- and thick-disc components derived in this work.

Component	σ_{v} (km s^{-1})	h_{r} (kpc)	z_0 (kpc)	$[\mathrm{Fe/H}]_{\mathrm{spec}}$
Thin disc	35.7 ± 1.0	7.3 ± 1.1	1.1 ± 0.2	-0.7 ± 0.05
Thick disc	50.8 ± 1.9	8.0 ± 1.2	2.8 ± 0.6	-1.0 ± 0.1

4 RESULTS

4.1 Kinematic and structural properties of the thin and thick discs

In this section, we present measurements for the kinematic and structural properties of the thin and thick discs. Properties of individual fields can be found in Table 2, while the average properties for both components can be found in Table 3.

4.1.1 Velocity lag and dispersion profiles

In this first section, we initially address the thin and extended discs of M31. In I05, the extended disc was identified as a stellar disc that, while appearing in many respects to be similar to the classical thin

Table 2. Kinematic properties of the thin- and thick-disc components.

Field	$v_{\mathrm{thin,lag}}$ (km s^{-1})	σ_{thin} (km s^{-1})	$v_{\mathrm{thick,lag}}$ (km s^{-1})	σ_{thick} (km s^{-1})	σ_{conf}	$[\mathrm{Fe/H}]_{\mathrm{thin}}$	$[\mathrm{Fe/H}]_{\mathrm{thick}}$
228Dis	6.8 ± 5.0	55.2 ± 3.2	-141.9 ± 7.5	41.2 ± 11.8	37.0	-0.8 ± 0.1	-1.0 ± 0.1
227Dis	-3.7 ± 10.8	68.7 ± 3.3	N/A	N/A	2.8	-0.7 ± 0.2	N/A
166Dis	-7.5 ± 6.9	48.9 ± 4.6	N/A	N/A	0.5	-0.8 ± 0.2	N/A
106Dis	11.6 ± 8.2	47.4 ± 5.2	-85.0 ± 8.2	52.5 ± 4.1	3.5	-0.9 ± 0.3	-1.0 ± 0.3
105Dis	-16.4 ± 7.2	32.0 ± 4.1	-54.8 ± 8.7	51.0 ± 5.2	4.0	-0.7 ± 0.2	-1.0 ± 0.2
224Dis	-34.4 ± 6.2	24.3 ± 2.5	-63.8 ± 10.2	55.0 ± 12.5	5.1	-0.9 ± 0.1	-1.1 ± 0.2
232DiS	-37.2 ± 3.0	35.0 ± 3.8	N/A	N/A	2.0	-0.8 ± 0.1	N/A
104Dis	-37.9 ± 6.5	30.0 ± 4.4	-114.3 ± 9.5	53.3 ± 7.2	9.0	-0.7 ± 0.2	-0.9 ± 0.1
220Dis	-12.5 ± 5.0	39.6 ± 2.9	-64.8 ± 12.1	54.7 ± 10.9	26.7	-1.1 ± 0.3	-1.6 ± 0.3
213Dis	-10.9 ± 3.2	31.9 ± 6.3	-80.5 ± 10.0	55.0 ± 8.8	39.2	-0.8 ± 0.3	-1.5 ± 0.3
102Dis	-18.8 ± 7.1	22.2 ± 5.2	-61.5 ± 11.6	48.1 ± 5.6	47.1	-0.9 ± 0.2	-1.0 ± 0.2
231Dis	4.7 ± 15.2	22.9 ± 4.2	-35.9 ± 7.8	53.4 ± 7.2	43.4	-0.9 ± 0.1	-1.1 ± 0.2
223Dis	-8.1 ± 5.9	20.1 ± 4.9	-55.7 ± 9.9	51.1 ± 6.8	14.7	-0.7 ± 0.2	-1.0 ± 0.3
101Dis	-16.2 ± 3.9	35.8 ± 5.8	-57.3 ± 8.6	44.9 ± 6.2	3.1	-1.1 ± 0.2	-1.3 ± 0.3
222Dis	-25.9 ± 4.8	33.6 ± 2.9	N/A	N/A	0.8	-0.7 ± 0.1	N/A
221Dis	-27.5 ± 5.5	35.0 ± 3.6	-121.2 ± 7.4	52.2 ± 6.3	27.1	-1.1 ± 0.2	-1.4 ± 0.2
50Disk	-16.9 ± 8.1	34.2 ± 5.9	-149.2 ± 13.2	42.3 ± 7.2	12.6	-1.0 ± 0.2	-1.2 ± 0.2
107Ext	-55.2 ± 6.9	24.8 ± 4.4	N/A	N/A	2.4	-1.0 ± 0.3	N/A
w11old	-55.1 ± 10.2	28.8 ± 5.6	N/A	N/A	1.4	-1.0 ± 0.3	N/A
167Hal	-72.6 ± 8.3	22.9 ± 5.4	-120.3 ± 12.2	35.1 ± 7.8	23.5	-0.9 ± 0.3	-1.0 ± 0.3
148Ext	-17.2 ± 7.0	41.3 ± 6.6	-154.5 ± 11.0	25.7 ± 5.1	28.2	-0.9 ± 0.3	-1.0 ± 0.2

disc, was a separate entity that was clumpy in terms of its structure and lagged behind the classical disc in terms of its kinematics. As we are limiting our study to one slice down the major-axis of M31, we do not attempt to comment on the global 'clumpiness' of this extended disc, but we return to the issue of the velocity lag and distinction from the thin stellar disc. As we have analysed the disc-frame velocities for all our fields using a rotation curve that differs from the one used in I05, it is useful for us to determine whether the increasing lag with respect to the classical thin disc is seen here also. In I05, they split their sample of 21 fields into an inner (with $R_{\rm proj} < 20$ kpc) and outer (with $20 < R_{\rm proj} < 30$ kpc) sample to determine the average properties of the disc and extended disc. For their inner (classical) disc sample, they calculated an average velocity for the disc in the disc lag frame of $v_{\rm lag} = -17.0\,{\rm km\,s^{-1}}$ and a dispersion of $\sigma_{\rm v} = 50.0\,{\rm km\,s^{-1}}$. In the outer (extended) sample, they calculated an average velocity of $v_{\rm lag} = -16.0\,{\rm km\,s^{-1}}$ and a dispersion of $\sigma_{\rm v} = 51.0\,{\rm km\,s^{-1}}$. If we perform the same analysis for our study, we find an average lag of $v_{\rm lag} = -14.8\,{\rm km\,s^{-1}}$ for our inner fields and $v_{\rm lag} = -25.5\,{\rm km\,s^{-1}}$ for our outer fields. However, we note that this value is calculated with the inclusion of fields 107Ext, w11old and 167Hal, which have very large lags of $v_{\rm lag} < -55\,{\rm km\,s^{-1}}$ compared with the other fields. We note that these fields are located slightly off the semimajor-axis (see Fig. 4) where our interpolated disc-frame velocities are subject to larger uncertainties. If we exclude these fields, we find an average lag of $v_{\rm lag} = -14.9\,{\rm km\,s^{-1}}$, very similar to our inner sample. We therefore conclude that there is a negligible difference in the lags of the classical and extended discs behind circular velocities. For these samples, we also calculate average dispersions of $\sigma_{\rm v} = 42.7$ and $30.0\,{\rm km\,s^{-1}}$, implying that the extended disc has a lower dispersion than the classical disc. However, in our inner sample, we are more likely to see residual contamination from the bulge and we also have a large proportion of fields for which we could not cleanly isolate the thick disc (~40 per cent compared with ~20 per cent in the outer sample). These factors may cause us to overestimate the dispersion of the disc in these regions. From these results, we therefore find no concrete reason to assume that the extended disc is a separate component from the classical disc and we treat these two components as one thin stellar disc in the remainder of our analysis.

By using the information from our Gaussian fits to the thin- and thick-disc components, we can comment on their global kinematic properties and discuss any variation in these properties with the radius. In Table 2, we show the peak velocities and velocity dispersions of both thin- and thick-disc (where applicable) components in each field, with associated errors from the GMM fits. Where both thin- and thick-disc components are detected, we compute the lag between the two components, $\Delta v = v_{\rm thin} - v_{\rm thick}$, and plot this lag as a function of radius in Fig. 8. The 14 fields for which a thick-disc component is reliably detected cover a range of radii from 15.2 to 39.6 kpc. In the top panel of Fig. 8, we can see that the lag between the two components does not appear to increase with distance from the centre of M31 and shows an average lag of $\langle \Delta v \rangle = 46.0\,{\rm km\,s^{-1}}$.

We also plot the dependence of the velocity dispersion, $\sigma_{\rm thin}$ and $\sigma_{\rm thick}$, for both components on the radius in the middle panel of Fig. 8. For the thin disc, we fit both a constant relation and a single power law to the data. The linear power law suggests a decrease in dispersion with radius, with a gradient of $-0.87\,{\rm km\,s^{-1}\,kpc^{-1}}$; however, this fit is not statistically better than a constant fit, with an average dispersion of $\sigma_{\rm thin} = 31.6 \pm 1.1\,{\rm km\,s^{-1}}$ (reduced χ^2 of 5.6 versus 5.2). We do the same for our thick-disc results and we find that a linearly decreasing profile where $\sigma_{\rm thick} = -0.8(\pm 0.2)R_{\rm proj} +$

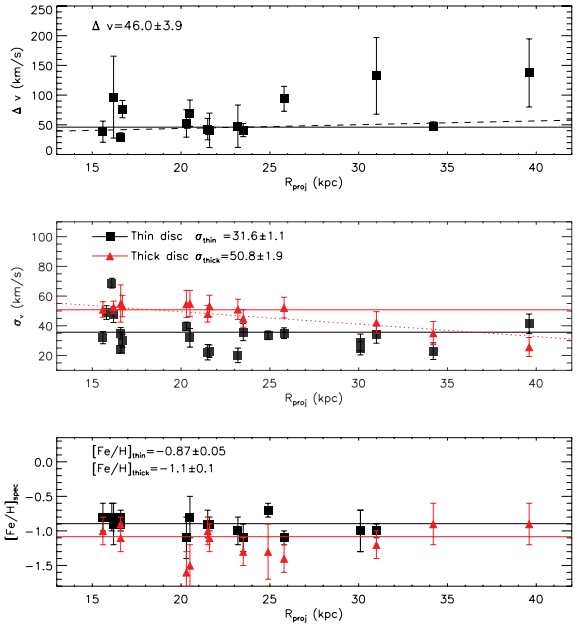

Figure 8. Top panel: the difference in velocity, Δv, between the thin- and thick-disc components as a function of the projected radius. This lag appears to be approximately constant as a function of the radius, with an average lag of $46.0 \pm 3.9\,{\rm km\,s^{-1}}$. There appears to be a slight increase in the lag in the outermost part; however, this is largely driven by fields that lie off the major-axis of M31 and therefore the velocities are less reliable. Middle panel: dispersion, $\sigma_{\rm v}$, of both thin- (black squares, solid line) and thick-disc (red triangles, dot–dashed line) components is plotted as a function of the projected radius. The thin disc appears to maintain a constant dispersion of $\sigma_{\rm thin} = 35.7 \pm 1.0\,{\rm km\,s^{-1}}$; however, the thick component appears to decrease somewhat at larger radii. Bottom panel: average spectroscopic metallicity of thin- and thick-disc components as a function of the projected radius. Neither component evolves with the radius.

$66.1(\pm 5.8)$ has a marginally better fit to the data than a fit with no evolution; however, the difference in negligible (reduced χ^2 of 1.2 versus 1.4) and deemed insignificant in a χ^2 significance test. Even if we were to accept this fit as preferred, we note that the two outermost fields situated at 34.2 and 39.6 kpc are perhaps the driving force in the decreasing dispersion seen in our thick-disc component. As these field are the farthest out in our survey, they also suffer from the greatest chance of halo contamination in our sample and therefore could be unreliable. If we exclude these final points from the fit, we find that $\sigma_{\rm thick}$ is best fitted with no evolution as a function of radius, with an average dispersion of $50.8 \pm 1.9\,{\rm km\,s^{-1}}$. We therefore conclude that our data cannot tell us anything reliable about the dependence of these kinematic properties on radius and allow us to merely calculate the average kinematics of both components.

4.1.2 Scalelength of the thin and thick discs

To determine the scalelengths of our two disc components, we need to calculate the number density of thin- and thick-disc stars within our DEIMOS field of view. There are two complications we must consider before we proceed. First, the two components are not completely distinct from one another and in all fields, we observe some overlap. Secondly, owing to our selection criteria (discussed in Section 3), we prioritize stars of certain colours and magnitudes above others and this must be considered when calculating densities on a field-by-field basis.

We determine the number of stars associated with the extended thin disc, n_s, in each of our fields by integrating the Gaussian we have fitted to this component. To determine the density of stars contained in the thin disc, we multiply n_s by the total number of available target stars within our DEIMOS field that fall within our selection criteria, n_t, and divide this by the total number of stars that were observed with our DEIMOS mask, n_o. We then subtract the density of background stars, n_b, which is computed from a number of fields on the edge of our survey region, that is, $\rho_* = n_s n_t / n_o - n_b$. To account for our prioritized selection technique, we perform this calculation separately for our priority A and priority B stars, and then combine these measurements. We repeat this calculation for the thick disc. We plot the results in Fig. 9, where we apply a weighted-least-squares exponential fit to our data points and determine $h_r = 7.3 \pm 1.1$ kpc for the thin disc and $h_r = 8.0 \pm 1.2$ kpc for the thick disc. Comparing these to previous calculations for the scalelength of the thin and extended discs, we find that the extended disc has a larger scalelength than the exponential thin disc (5.1 ± 0.1 kpc, I05). The value of 7.3 kpc that we derive is slightly higher than that derived in I05 of 6.6 ± 0.4 kpc and with much larger error bars, but the two are consistent within their 1σ uncertainties. The difference between the two values can be attributed to two factors. First, in I05, they included fields from the NE of the galaxy, plus fields located away from the major-axis, where we have sampled fields solely from the SW major-axis. Secondly, in I05, they did not fully address any biases that may have been introduced by our two-tiered prioritization system. Finally, we note that the thick disc appears to be more radially extended than either the thin or the extended disc, although it is consistent with the scalelength of the extended disc within its 1σ errors.

In previous work, YD06 measured the scalelengths of 34 edge-on disc galaxies using a photometric fitting technique and found that the scalelengths of the thick discs were larger than those of the thin discs by a factor of $\sim$1.3. We plot their results in the left-hand panel of Fig. 10 and overlay a linear relation with a gradient of 1.3. We add to this our results for M31, using an average value for the thin disc from the range of scalelengths derived for the thin and extended discs (5.1–7.3 kpc) of 6.3 kpc, and our calculated value of 8.0 kpc. We also overplot the result for the MW (using Jurić et al. 2008 values of 2.6 and 3.6 kpc for the thin and thick discs, respectively) and note that M31 sits in excellent agreement with this relation.

4.1.3 *Inferring the scaleheights of the thin and thick discs*

Owing to the inclination of M31, we are unable to measure the scaleheight of either the thin- or the thick-disc components directly. No photometric excess above a typical bulge or extended disc profile is observed when performing minor-axis star counts (Irwin et al. 2005), suggesting that these components dominate the surface profile out to large radii. In order to infer probable scaleheights for both components, we make use of the properties of the 34 edge-on galaxies measured by YD06. As the scalelengths and scaleheights of both the thin and thick discs in each of these galaxies were derived, it is possible for us to search for a relation between the scalelength, h_r, and scaleheight, z_0, of each component. In the middle panel of Fig. 10, we plot h_r versus z_0 for the YD06 sample as well as for the MW (Ivezić et al. 2008), and fit it with a linear relation, on which we force an intercept of (0, 0). We find that the data are well fitted with a gradient for this relation of 0.18 ± 0.04, though there is significant scatter beyond $\sim$9 kpc. From this, we deduce $z_0 = 1.1 \pm 0.2$ kpc for the M31 extended disc (using $h_r = 7.3$ kpc). We repeat this for the thick disc (shown in the right-hand panel of Fig. 10) and find that these values are well fitted with a linear relation of gradient 0.35 ± 0.06, giving us $z_0 = 2.8 \pm 0.6$ kpc for the M31 thick disc. If these values are correct, then not only are the discs of M31 more radially extended than those of the MW by a factor of $\sim$2–3, but they are also significantly thicker.

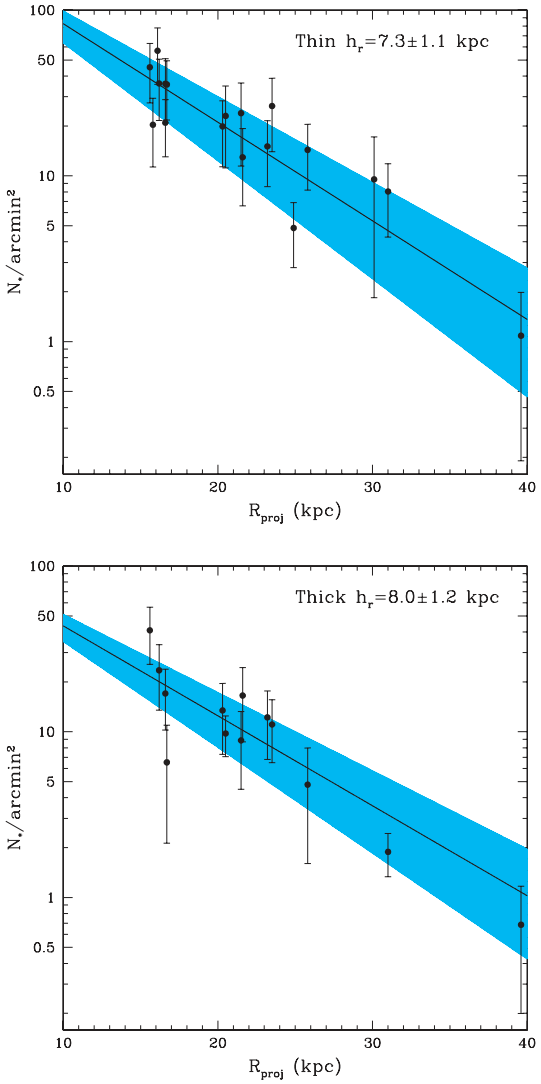

Figure 9. Top panel: plot of the density of stars (N_*/arcmin^2) in the thin disc against R_{proj}. The densities are calculated by first separating our sample by their target prioritization (A or B, see Section 3), then counting all stars with $v_{thin} > v_{lag} > v_{thin} + 2\sigma_{thin}$ and multiplying these values by 2 (i.e. assuming the distributions are symmetric) for both prioritizations. We then calculate $\rho_* = n_s n_t / n_o - n_b$ and combine these results from priority A and B. Fitting an exponential profile to these points, we deduce $h_r = 7.3 \pm 1.1$ kpc. The solid line represents the best fit to the data from a weighted-least-squares routine and the shaded region indicates the 1σ errors from the fit. Bottom panel: as above, for the thick disc. Here we count all stars with $v_{thick} - 2\sigma_{thick} > v_{lag} > v_{thick}$ and multiply these values by 2 again . Fitting an exponential profile to these points, we deduce $h_r = 8.0 \pm 1.2$ kpc.

4.1.4 *Contrast of the thin and thick discs*

In the previous sections, we have derived the density in each field of both our components as a means to determine the scalelengths. We now use these densities to work out how much of the total (disc-related) stellar population is contained within each

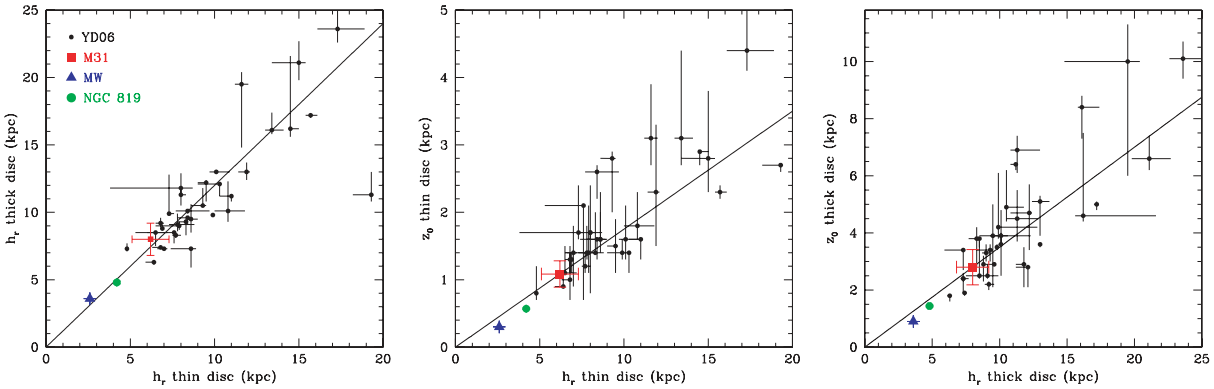

Figure 10. Here we compare the scalelengths of the thin and thick discs in M31 to those of other galaxies with observed thick discs in order to infer their scaleheights. Left-hand panel: here we plot thin-disc scalelengths against thick-disc scalelengths for 34 external galaxies (YD06) as black points and overplot the same measurements for the MW (blue triangle). We fit a linear relation to these points with a gradient of 1.3. We plot our result for M31 as a red square and it is in excellent agreement with this relation. Middle panel: here we plot a scaleheight, z_0, against the scaleheight for the thin disc of the YD06 sample plus the MW and derive a best-fitting linear function with a gradient of 0.17. From this, we can estimate a scaleheight for the M31 thin disc of 1.1 ± 0.2 kpc, which we overplot on the relation as a red square. Right-hand panel: we now plot the same, but for the thick disc, and find a best-fitting gradient of 0.35, and therefore infer a scaleheight for the thick disc in M31 of 2.8 ± 0.6 kpc, which is overplotted as a red square.

component. There are several caveats to such a comparison that should be mentioned. First, our sampling of the field is likely to have an effect on our field-to-field estimates of the stellar density (which we discuss further in Section 5). Secondly, as the disc is not observed edge-on, we are measuring a 2D projection of the densities which is difficult to interpret. We also note that the measurement errors associated with the densities of each field (shown in Table 4) are significant (of the order of ∼50 per cent).

With this in mind, we find that, on average, the thick-disc component accounts for 35 per cent of the total stellar density, with an interquartile range (IQR) of ±10 per cent. In the MW, we know that the thick disc contributes to ∼10 per cent of the stellar density in the solar neighbourhood and accounts for approximately one-third of the *total* disc mass (Jurić et al. 2008; Schönrich & Binney 2009a), comparable to what we derive here.

Table 4. Field-by-field densities of thin- and thick-disc stars.

Field	$\rho_{*\mathrm{thin}}$ (N_*/arcmin^2)	$\rho_{*\mathrm{thick}}$ (N_*/arcmin^2)
228Dis	57.6 ± 22.3	N/A
227Dis	56.9 ± 22.3	N/A
166Dis	20.4 ± 9.4	N/A
106Dis	36.2 ± 15.3	23.6 ± 10.5
105Dis	45.3 ± 18.6	41.0 ± 16.3
224Dis	20.1 ± 8.4	17.1 ± 7.1
232DiS	35.9 ± 15.7	N/A
104Dis	35.7 ± 14.6	6.6 ± 4.5
220Dis	19.9 ± 8.9	13.5 ± 6.4
213Dis	23.0 ± 12.2	9.8 ± 3.0
102Dis	24.0 ± 12.8	8.9 ± 4.5
231Dis	13.0 ± 6.6	16.6 ± 8.1
223Dis	15.1 ± 6.7	12.2 ± 5.6
101Dis	26.5 ± 12.9	11.1 ± 4.8
222Dis	4.9 ± 2.1	N/A
221Dis	14.4 ± 6.4	4.8 ± 3.3
50Disk	8.1 ± 3.9	2.0 ± 0.6
107Ext	9.6 ± 7.8	N/A
w11old	9.0 ± 6.5	N/A
167Hal	1.3 ± 0.8	0.8 ± 0.5
148Ext	1.1 ± 0.9	0.7 ± 0.5

From our calculated contrasts and individual density profiles for the thin and thick discs, we can estimate the mass contained within the thick-disc component using values for the mass of the thin disc from the literature. From our analysis above, we have determined that the thick disc contributes 35 ± 10 per cent of the *total* stellar density, meaning the thick-to-thin-disc density ratio is of the order of 55 ± 15 per cent. We can also estimate this fraction by integrating our stellar density profiles (Fig. 9) over the limits of our data and from this we calculate a thick-to-thin-disc density ratio of ∼65 per cent, which is in good agreement with our contrast estimate. If we assume that both discs are composed of similar stellar populations, then we can set the mass ratio between the discs to be equivalent to the density ratio. In Yin et al. (2009), they quote a total mass for the thin stellar disc of $M_{*,\mathrm{thin}} = 5.9 \times 10^{10}\,\mathrm{M}_\odot$, calculated from the mass models of Widrow, Perrett & Suyu (2003) and Geehan et al. (2006). From this we estimate that the total mass of the M31 thick disc lies in the range $2.4 \times 10^{10} < M_{*,\mathrm{thick}} < 4.1 \times 10^{10}\,\mathrm{M}_\odot$. As we are unable to determine the full radial and underlying luminosity profile for the thick disc, these values are obviously prone to large errors introduced by our simplifying assumptions, and the mass of the thick disc may be lower than our quoted range. For example, if we just compare the number of stars we detect in the thin disc throughout our entire sample with the number of stars we detect in the thick disc by integrating the fitted Gaussians in Fig. 6, we find a thick-to-thin-disc ratio of 20 per cent. If we assume this value for the ratio of the masses between the components, our lower limit on the thick disc is reduced to $M_{*,\mathrm{thin}} = 1.2 \times 10^{10}\,\mathrm{M}_\odot$. A future study of the thick disc which includes fields from the entirety of our survey will help us to better constrain both the radial profile and the mass of this component.

4.2 Spectroscopic metallicities

In this section, we present the spectroscopic values of [Fe/H], both for individual stars and for the composite spectrum of each component. Measuring individual metallicities from the Ca II triplet for the stars in our survey, with S/N typically between 5–15 Å^{-1}, is quite problematic. In Battaglia et al. (2008), they show that the 'best-case' errors in measuring the EWs of the Ca II lines, ΔEW, scale with

S/N as

$$\Delta\mathrm{EW} = \frac{\sqrt{1.5 \times \mathrm{FWHM}}}{\mathrm{S/N}}, \quad (3)$$

assuming no contamination from residual sky lines and no covariance noise, where FWHM is the full width at half-maximum of the Ca II lines which is typically 2–3 Å. Using this equation, we can determine the average errors in [Fe/H] for stars in our sample at different S/N, and we find that for spectra with S/N of 5, 8 and 10 $\mathrm{Å}^{-1}$, the errors in their calculated metallicity are of the order of 0.6, 0.4 and 0.3 dex, respectively. To demonstrate the effects of these large errors on the metallicity distribution function (MDF) of our sample, we present histograms of the individual spectroscopic metallicities for three quality cuts, one at S/N $\geq 10\,\mathrm{Å}^{-1}$ (left-hand panel), one with S/N $\geq 8\,\mathrm{Å}^{-1}$ (middle panel) and one with S/N $\geq 5\,\mathrm{Å}^{-1}$ (right-hand panel) in Fig. 11. In both plots, the blue hatched histogram represents our thin-disc sample and the filled red histogram represents our thick-disc population. For our higher quality spectra, we calculate a median metallicity for the thin disc of [Fe/H] $= -0.9$ with a dispersion of 0.4 dex (from the IQR). For our thick-disc population, we calculate a median of [Fe/H] $= -1.0$ also with a dispersion of 0.4 dex. We note that the distributions of both populations deviate from a Gaussian distribution, with a kurtosis of -0.6 and -0.3 for the thin and thick discs, respectively, implying a broad peaked distribution, with narrow tails. Both distributions are skewed towards lower metallicity with skewness $\alpha = -0.4$ and -0.3 for the thin and thick discs, respectively. For our lowest S/N cut, however, much of this information is lost. While the median [Fe/H] remains very similar to [Fe/H] $= -1.0$ for the thin disc and to [Fe/H] $= -1.1$ for the thick disc, the distributions begin to broaden, with dispersions of 0.5 dex for both populations, and present almost no skew ($\alpha = -0.1$ and -0.2 for the thin and thick discs, respectively). This shows that by including data with larger measurement errors, we wash out our MDF considerably and lose any meaningful information. As a sanity check, we compare the MDF for all stars with S/N $\geq 10\,\mathrm{Å}^{-1}$ with the one for stars with S/N $\geq 15\,\mathrm{Å}^{-1}$ and find both the median values of [Fe/H] and general distributions to be comparable. We note that by requiring such a high S/N cut on our individual measurements of [Fe/H], we bias our sample towards more metal-rich stars as these will have intrinsically stronger Ca II lines.

Owing to the large errors associated with these measurements, this analysis provides a crude indication of the metallicities of both discs and so to get a more accurate estimate of the average metallicities of both populations we construct composite spectra for both components (using both the 2σ and Gaussian velocity cuts) by co-adding the individual spectra of all stars with S/N $> 3\,\mathrm{Å}^{-1}$, weighted by their S/N values. The resulting S/N of the composite spectra is much greater than the individual spectra (S/N $\sim$ 60–100 compared with S/N $\sim$ 3–25), allowing a better fit to the Ca II lines. We use a cut of S/N $> 3\,\mathrm{Å}^{-1}$ as below this the velocity uncertainties of our stars begin to significantly increase (as discussed in Section 3). As we shift all spectra to the rest frame before co-adding, including spectra where the velocity is uncertain could smear out the Ca II lines, resulting in an overestimate of [Fe/H] for the composite. We note that the results from our composites are only indicative of an average metallicity for each component and can tell us nothing about the metallicity dispersion for the discs. We display the resulting composites in Fig. 12. The top two panels show the thin- and thick-disc spectra for the 2σ velocity cuts, while the bottom two panels show the same, but for the Gaussian velocity cuts. In the case of the 2σ cuts, our thin-disc composite spectrum comprises 511 stars that match our kinematic and quality criteria, while our thick-disc composite spectrum comprises 78 stars. For our Gaussian cuts, these numbers fall to 380 and 52 stars, respectively. We find an offset of the order of 0.2 dex between the thick- and thin-disc components for the 2σ cuts, with the thick disc being more metal poor at [Fe/H] $= -0.9 \pm 0.1$ compared with [Fe/H] $= -0.7 \pm 0.05$ for the thin disc, inconsistent within their respective 1σ errors. For our Gaussian cuts, we find the thick disc to be more metal poor, giving us a larger difference in metallicity between the two components of 0.3 dex (with [Fe/H] $= -1.0 \pm 0.1$ for the thick disc compared with [Fe/H] $= -0.7 \pm 0.05$ for the thin), although the two results for the thick disc are consistent within their 1σ errors. We also note that we are liable to experience non-negligible thin-disc contamination of our thick-disc component, which could cause us to overestimate the average [Fe/H], so the true difference could be larger still. We note that these results are consistent with performing the same analysis on composites constructed from spectra with S/N $> 10\,\mathrm{Å}^{-1}$.

Finally, the continuum fit to the third line in our composite spectra, particularly for our thick-disc selection, gives us some cause for concern. Could this metallicity difference we derive be driven by

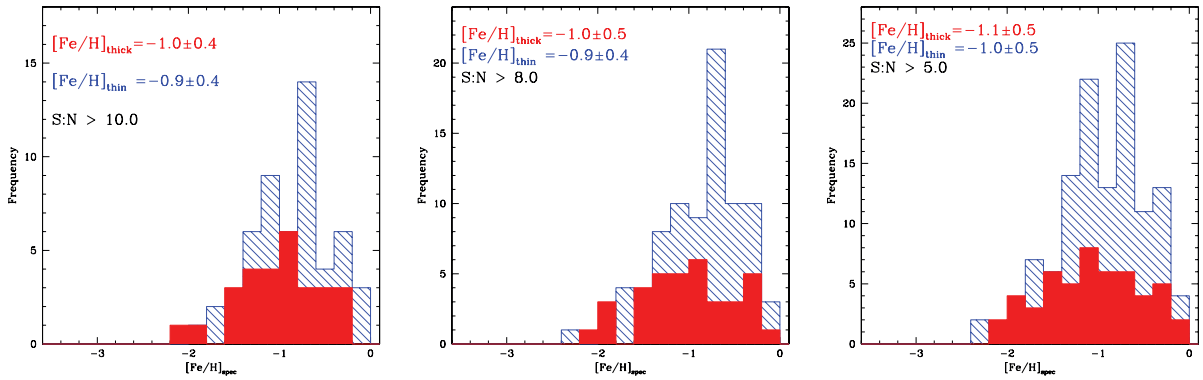

Figure 11. Here we display the spectroscopic MDF for all stars in our thin- and thick-disc components (shown as the blue hatched and red solid histograms, respectively). In the left-hand panel, we show the MDF using all stars for which metallicities can be reliably measured (i.e. S/N $\geq 10\,\mathrm{Å}^{-1}$), and the middle and right-hand panels apply lower quality cuts (S/N $\geq 8\,\mathrm{Å}^{-1}$ and S/N $\geq 5\,\mathrm{Å}^{-1}$, respectively). For our lower S/N cuts, we note that the median [Fe/H] values for both populations remain similar and the dispersions (IQR) begin to increase, losing some of the detail of the shape of the MDF. In all cases, the median [Fe/H] of the thick disc is more metal poor than that of the thin disc by $\sim$0.1 dex.

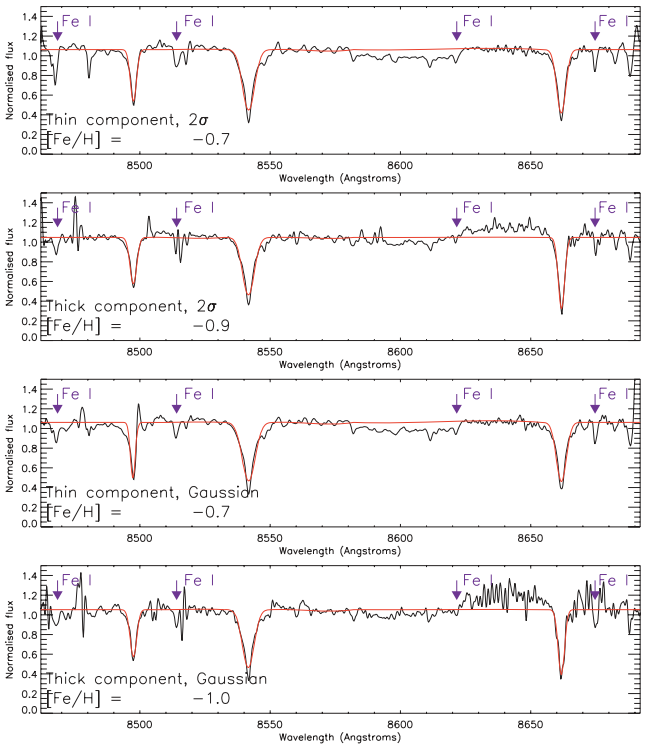

Figure 12. Composite spectra of both the thin-disc and thick-disc components, using both 2σ (top panel) and Gaussian (lower panel) cuts to isolate the thick-disc component. The composite spectra are constructed from stars within the selection regions that possess a S/N $\geq 3.0\,\text{Å}^{-1}$. We find that the average metallicity for the thin-disc component is more metal rich than the thick-disc component by 0.2–0.3 dex. These results are consistent with composites formed from spectra with S/N $\leq 3\,\text{Å}^{-1}$ and with our field-by-field metallicity estimates (Fig. 8). We also show the locations of a number of Fe I lines present in these spectra.

poor continuum fitting in this region of the spectrum? To investigate this, we analyse [Fe/H] for the thin and thick discs again, using solely the first two lines (Ca II$_{8498}$ and Ca II$_{8542}$). In the case of our simple 2σ cut, this narrows our difference in metallicity slightly from 0.2 to 0.15 dex, with [Fe/H] $= -0.85 \pm 0.1$ compared with [Fe/H] $= -0.7 \pm 0.05$ for the thick and thin discs, respectively. However, in the case of our Gaussian cuts, which are arguably less affected by cross-contamination between the components, the metallicity difference of 0.3 dex persists.

We also perform this composite analysis on a field-by-field basis. The results of this analysis, shown in Table 2, are again less accurate than our overall composite, but they suggest a similar offset in metallicity exists in the thin- and thick-disc components in each field. We plot this result as a function of radius in the lower panel of Fig. 8. We find no evidence for any evolution of metallicity with radius.

A slight concern in ascertaining the metallicity of a population from a composite spectrum arises from inaccuracies in the estimate that come from combining spectra with different effective temperatures and V-band magnitudes, as the derived metallicities are weakly dependent on the apparent V-band colours of the stars. The rms dispersion in the V-band magnitudes within our sample is small (<0.5 mag for both the thin and thick discs) as we are sampling only a small region of the tip of the RGB, so the error introduced by this effect will be very small. However, to further assess this, we separate our thin- and thick-disc spectra into bins of 0.2 mag in the V band and create composite spectra for each bin, measuring the metallicity of each. We show a sample of these spectra in Fig. 13, labelled with the metallicity and average V-band magnitude. The typical errors in metallicities determined for these composites range from 0.1 to 0.3 dex. What we see is that the composite thick-disc spectrum in each bin is more metal poor than the corresponding thin-disc composite. We also find that the average metallicities for both the thin and the thick discs agree with those that we derived from the composites for the entire sample.

4.3 Photometric metallicities

We inspected the photometric metallicities of our sample using the Dartmouth isochrone models (Dotter et al. 2008). We select an age of 8 Gyr as the work of Brown et al. (2006) suggests that the age of the disc in these outer regions varies between 4–8 Gyr. We use an α-abundance of [α/Fe] $= +0.2$ as it has been shown in various works (e.g. Reddy, Lambert & Allende Prieto 2006; Alves-Brito et al. 2010) that the α-enhancement of thin or extended stellar disc populations typically ranges between [α/Fe] $= +0.0$ and $+0.2$. We then interpolate between these isochrone models for every star within our sample to determine its metallicity. We can then compare the MDFs for our thin- and thick-disc samples, selected by both the 2σ and Gaussian cuts discussed above. The results of this are shown in the left-hand panel of Fig. 14. This figure shows us that when using this set of isochrones, the MDFs of both populations trace each other remarkably well. We calculate a median metallicity for each component and find [Fe/H]$_{\text{thin}} = -0.79$ and [Fe/H]$_{\text{thick}} = -0.80$, both with IQRs of 0.2 dex. Neither population has a Gaussian distribution, with positive kurtosis of $+2.2$ for both MDFs (i.e. more peaked, with broader tails), and both populations are skewed towards lower [Fe/H] with $\alpha \sim -1.2$ for both discs. From this analysis, one might conclude that the two discs are chemically indistinguishable. This is in contrast to our findings from the combined spectra in Section 4.2 where we find an offset in the average metallicities of thin- and thick-disc components of 0.2 dex. As our photometric data are not deep enough to detect the main sequence turn-off (MSTO) of these fields, we are exposed to the age–metallicity–[α/Fe] degeneracy problem. If we analyse our data with isochrones of different ages and abundances, we find that the individual metallicities we measure change. Increasing the age by 2 Gyr has the effect of decreasing [Fe/H] of a star by ∼0.05 dex on average (shown in the middle panel of Fig. 14), and increasing the abundance from [α/Fe] $= +0.2$ to $+0.4$ reduces [Fe/H] by ∼0.1 dex (right-hand panel, Fig. 14). The dispersions, kurtosis and skew remain largely unchanged by these variations. These findings demonstrate that it may be difficult to discern slight differences in metallicity (such as 0.2 dex measured in Section 4.2) using photometric isochrones without knowing the ages and/or α-abundances of the thick and thin discs. Studies of the thin and thick discs in the MW have shown that the thick disc is both older and more α-enriched than the thin disc (Reddy et al. 2006; Alves-Brito et al. 2010), and many of the formation scenarios of thick discs suggest this could be true for thick discs in general, including M31. Such differences would certainly affect our derived values of [Fe/H] for both discs.

5 DISCUSSION

In this section, we discuss our findings and comment on the morphology of this thick component. First, we compare our findings with an expected thin- plus thick-disc population inclined to us

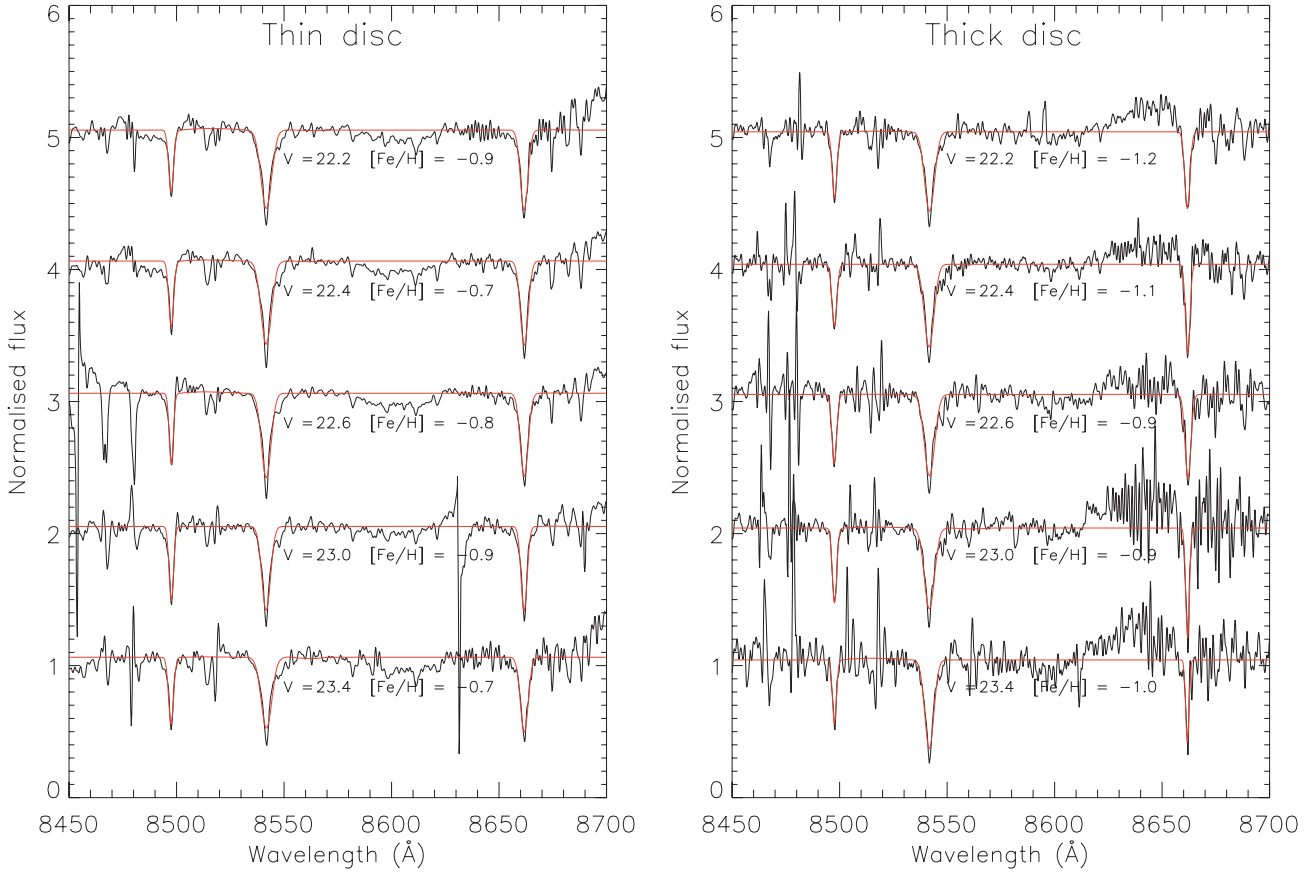

Figure 13. Composite spectra of our thin (left-hand panel) and thick (right-hand panel) disc samples, binned in V-band magnitude. Each bin spans 0.2 mag. We see that in each case, the thick disc is more metal poor than the thin disc by ∼0.2 dex. The errors in the values of [Fe/H] for these composites range from 0.1 to 0.3 dex.

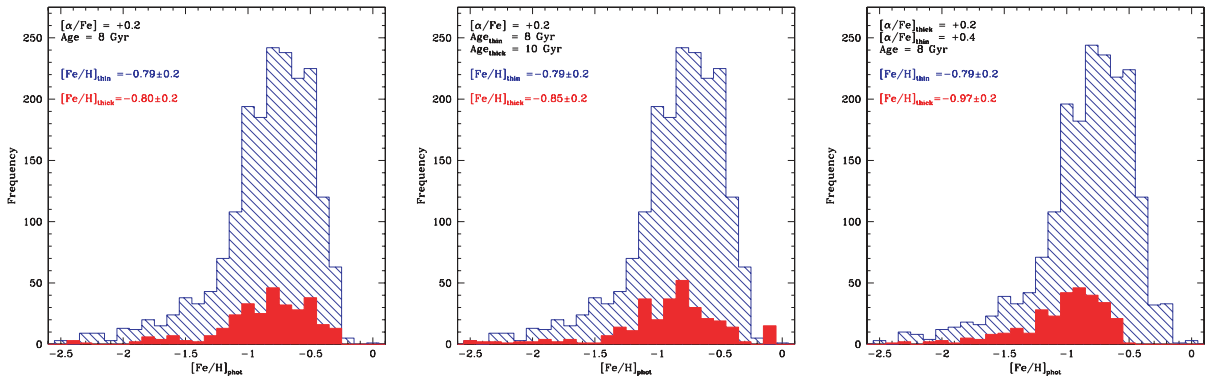

Figure 14. Photometric MDFs derived from Dartmouth isochrones of varying age and [α/Fe] (Dotter et al. 2008) for the thin- and thick-disc components (shown as blue hatched and red filled histograms, respectively) as defined by our 2σ cuts. Left-hand panel: analysis of [Fe/H] for the thin and thick discs using [α/Fe] = +0.2 and an age of 8 Gyr. We detect no significant differences between the two populations, calculating the median [Fe/H] and [Fe/H]$_{\rm thick} = -0.8 \pm 0.2$. Middle panel: increasing the age of isochrones used to calculate the metallicity for the thick disc from 8 to 10 Gyr. An offset of ∼0.05 dex in the average [Fe/H] of the two components is observed, with median [Fe/H]$_{\rm thick} = -0.85$. The dispersion remains the same as before. Right-hand panel: increasing [α/Fe] for the thick disc from +0.2 to +0.4. An offset of ∼0.1 dex between the median metallicities of the populations is now observed, with [Fe/H]$_{\rm thick} = -0.93$.

along the line of sight by 77°, by creating a model of a galaxy with a thin/extended disc with similar properties to those of M31 that has an additional thick-disc component and analysing it in the same way as our data. We then compare the M31 thick disc to the MW and the YD06 sample of thick discs. Finally, we comment on the possible formation mechanisms for this component.

5.1 Comparison with a thin- plus thick-disc model

To lend confidence to our defining the lagging component we isolate in the above analysis as a thick disc, we create a simple kinematic model of a galaxy with properties similar to those of a MW-type galaxy, which has both a thin and a thick stellar disc, and analyse

this in the same manner as our data. This is done as follows: first, we create a thin stellar disc of 9×10^6 stars, randomly generating radius for each, assuming the stars are distributed in an exponential disc with a scalelength equal to that of M31 (6.6 kpc, I05). We assign each particle with a velocity randomly drawn from a Gaussian population centred on $0\,\mathrm{km\,s^{-1}}$ with a velocity dispersion of $25\,\mathrm{km\,s^{-1}}$ in the disc frame. We repeat this for our thick-disc component, assuming a thin-to-thick-disc density ratio in M31 that is equal to that measured in the solar neighbourhood of 9:1 (Just & Jahreiß 2010), giving 1×10^6 stars, and we use a thick-disc scalelength of 8.0 kpc, as determined above. For the velocities, we assume the thick disc lags behind the thin one by $50\,\mathrm{km\,s^{-1}}$ and has the same velocity dispersion as the MW thick disc, $\sigma = 40\,\mathrm{km\,s^{-1}}$ (Ivezić et al. 2008). We also generate vertical heights within the discs for both thin- and thick-disc populations, assuming MW scaleheights for the discs (300 and 1000 pc for the thin and thick discs, respectively, Ivezić et al. 2008), *I*-band magnitudes between $25.0 \geq I \geq 20.3$ (0.1 mag brighter than the tip of the RGB in M31) and angular positions within the disc. We then convert our disc-frame velocities into heliocentric velocities using the H I rotation curve of Chemin et al. (2009). Finally, we interpret this model in the same way as our data, by rotating it into the coordinate system of M31 as observed from the MW [with the inclination and position angle (PA) as discussed in Section 3] and subtracting off the assumed disc velocity at that position by interpolating each of our model stars into our average disc velocity map (Fig. 3).

From this model data set, we select stars as we would select targets to observe when designing DEIMOS masks, requiring them to have *I*-band magnitudes between $22.0 \geq I \geq 20.5$. We then randomly select the same number of stars as is observed at each field location and make velocity histograms in the disc lag frame for each field. We then analyse these distributions with the same GMM technique described in Section 3.1, using a LRT to determine whether the distribution of each model field is best fitted by a single thin-disc component or a double thin-disc + thick-disc component. This procedure is repeated 100 times, allowing us to compute the average velocities and dispersions for each component plus sampling errors which we tabulate in Table 5. In our final 100 samples, the thick disc is detected in 15 of the 21 fields on average. The fact that we do not see the thick-disc component in all our model fields implies that the non-detections in our data are an effect of our sampling of the DEIMOS fields rather than the component being absent in these fields. We show the histograms and best-fitting Gaussians for three of these realizations compared with our data in Fig. 15.

We now assess how both the lag between components and the dispersions of each component evolve with radius for our model data set, and how accurately we can recover these values from our model. In Fig. 16, we plot these values for our model (black circles) alongside the values we obtained from our data (red squares) and fit the evolution of the model results with linear functions as before. In the top panel, we show the measurement of Δv for our model fields as a function of the projected radius. The model results show no evolution of Δv with radius, recovering an average lag across all fields of $48.9 \pm 6.7\,\mathrm{km\,s^{-1}}$, which is similar to the constant lag of $50\,\mathrm{km\,s^{-1}}$ implemented in our model.

Next, we compare the evolution of the disc dispersions for our model with the data, shown in the middle and lower panels of Fig. 16. The model thin disc is best fitted with a constant relation, giving an average lag of $\sigma_{\mathrm{thin}} = 21.5 \pm 1.7\,\mathrm{km\,s^{-1}}$, very close to the input of $25.0\,\mathrm{km\,s^{-1}}$. For the thick-disc dispersion, σ_{thick}, the measured dispersion in the model scatters about a mean dispersion of $\sigma_{\mathrm{thick}} = 38.8 \pm 2.4\,\mathrm{km\,s^{-1}}$, with no evidence of evolution with radius.

Finally, we can use our model to get a handle on how accurate our estimates of the scalelength of the M31 discs might be. We use the same MC technique as given above to calculate the density of stars in each component in our model fields 100 times and then we compute the average density from these results. These results are shown in Table 6, and the errors represent the dispersion of the densities computed in each field. We then plot the densities as a function of radius for the thin and thick discs (shown in Fig. 17), and fit the result with an exponential profile to determine the scalelength. For the thin disc, we calculate $h_{\mathrm{r}} = 6.2 \pm 0.8$ kpc, which is

Table 5. Average kinematic properties of model fields from 100 MC realizations.

Field	v_{thin} (disc frame, $\mathrm{km\,s^{-1}}$)	σ_{thin} ($\mathrm{km\,s^{-1}}$)	v_{thick} (disc frame, $\mathrm{km\,s^{-1}}$)	σ_{thick} ($\mathrm{km\,s^{-1}}$)
228Mod	11.4 ± 5.0	19.2 ± 8.0	-50.0 ± 8.9	38.3 ± 8.1
227Mod	-1.7 ± 0.6	25.5 ± 10.8	-37.1 ± 15.6	46.3 ± 12.4
166Mod	-3.4 ± 2.1	25.9 ± 7.3	-46.3 ± 9.1	43.0 ± 13.4
106Mod	-4.4 ± 3.2	25.9 ± 8.2	-54.3 ± 14.1	42.8 ± 9.3
105Mod	-2.1 ± 1.2	22.0 ± 9.4	-54.6 ± 13.8	39.4 ± 12.8
224Mod	-2.7 ± 1.9	23.1 ± 9.9	-40.2 ± 9.2	42.3 ± 10.3
232Mod	-3.1 ± 2.7	21.8 ± 8.2	-45.9 ± 12.2	41.2 ± 13.2
104Mod	-2.5 ± 1.7	22.8 ± 10.2	-57.6 ± 14.4	43.0 ± 11.0
220Mod	-7.0 ± 3.8	21.1 ± 10.3	-62.9 ± 8.7	36.2 ± 10.4
213Mod	-8.1 ± 4.3	19.5 ± 9.9	-55.1 ± 13.2	32.2 ± 13.9
102Mod	-3.5 ± 2.7	20.6 ± 8.9	-49.1 ± 7.9	34.9 ± 12.4
231Mod	-3.7 ± 2.2	19.4 ± 7.4	-49.6 ± 12.3	33.2 ± 9.3
223Mod	-1.8 ± 1.1	20.8 ± 7.2	-56.1 ± 11.7	36.7 ± 8.8
101Mod	1.9 ± 1.3	22.3 ± 7.0	-64.1 ± 11.2	38.4 ± 10.8
222Mod	-0.1 ± 1.2	19.9 ± 6.6	-51.3 ± 12.6	34.8 ± 11.0
221Mod	3.9 ± 2.3	19.9 ± 8.6	-46.2 ± 7.0	38.1 ± 11.1
50Mod	4.2 ± 2.5	17.9 ± 8.2	-42.2 ± 15.5	33.5 ± 12.6
107Mod	5.1 ± 2.7	17.5 ± 7.7	-57.1 ± 11.6	40.4 ± 12.9
w11Mod	4.7 ± 1.1	19.5 ± 6.8	-63.1 ± 10.4	43.4 ± 10.5
167Mod	2.0 ± 0.7	22.5 ± 5.7	-52.2 ± 8.6	41.6 ± 9.7
148Mod	-1.2 ± 1.5	25.2 ± 6.8	-53.2 ± 9.7	36.5 ± 10.3

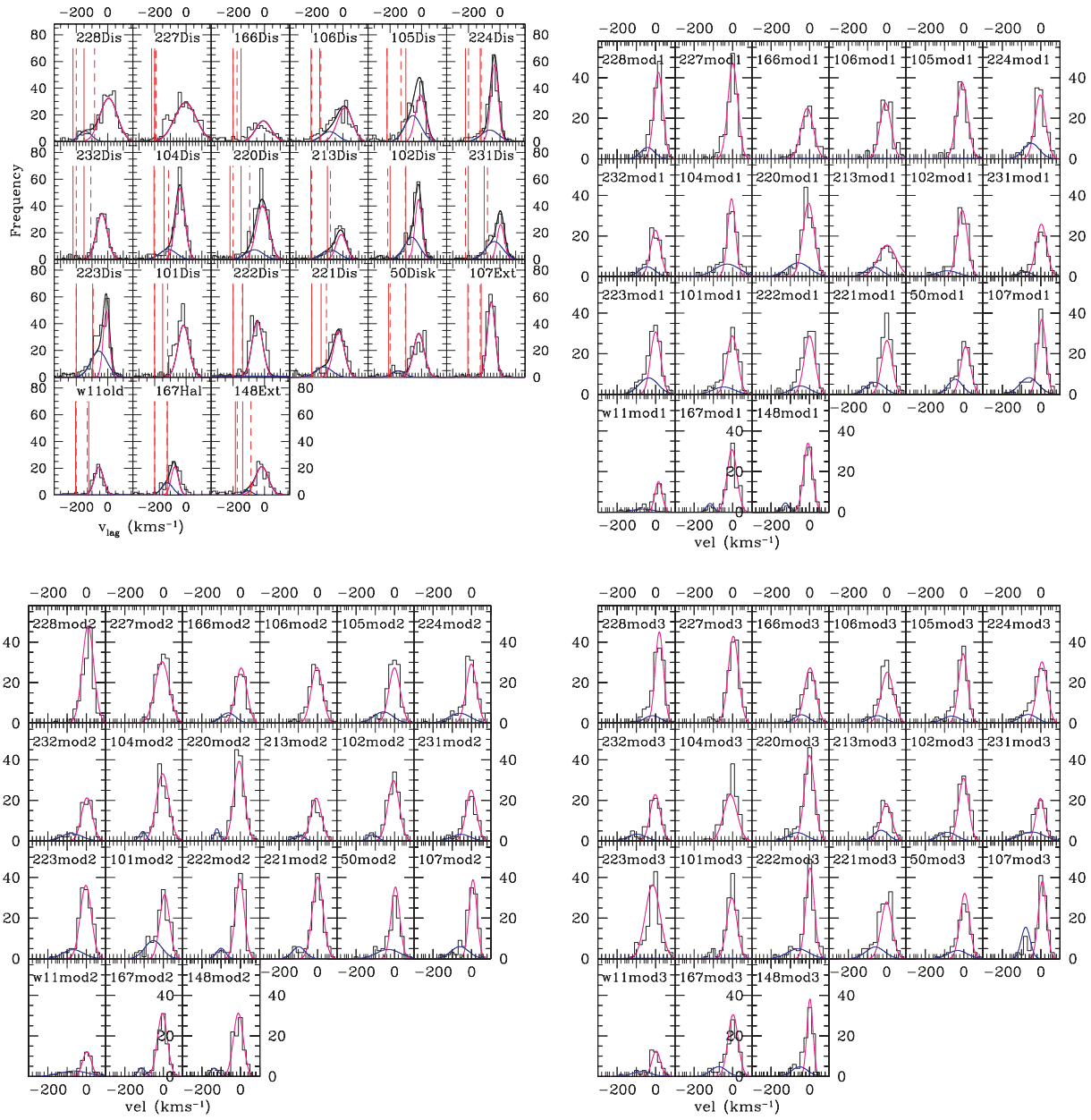

Figure 15. A comparison of the data (top left-hand panel) with three realizations of parsing our thin- plus thick-disc model through the same analysis as our data, selecting stars from the same regions as the data. It can be seen that the model data resemble the actual data very closely and that non-detections are likely an effect of sampling.

consistent with our input of 6.6 kpc, and for the thick disc, we compute $h_r = 7.8 \pm 0.9$ kpc, consistent with our input of 8.0 kpc. The shaded regions indicate the 1σ uncertainties from the fit. These results suggest that our observationally derived scalelengths for the thin and thick discs are a good indicator of their true scalelengths.

5.2 Comparison to the MW and 'edge-on' thick discs

Now that we have characterized the radial profile, kinematics and metallicity of the thick disc in M31, we are able to compare it to the properties of other thick discs that have been observed in the Universe. We shall begin with the most-well-studied thick disc currently known – that of our own Galaxy. Given that these two galaxies are relatively close to one another (separated by 785 kpc), and have similar morphologies (both large spiral galaxies), comparisons between the MW and M31 are often made. But for all their apparent similarities, these two galaxies are quite different from one another. Work by Hammer et al. (2007) has shown that the MW is quite different in terms of its structure and evolutionary history from the majority of local spiral galaxies, whereas M31 is actually quite 'typical', so these differences are perhaps unsurprising. In this work, we have demonstrated that the scalelengths of the M31 discs are larger than those of the MW by a factor of ∼2, as shown in Fig. 10. Given that we derive the scaleheights of the M31 discs from these scalelengths, this results in scaleheights in M31 that are of the order of approximately three times as thick as those of the MW. However, we note that as we calculate scaleheights for the M31 disc based on a relation determined from disc galaxies that

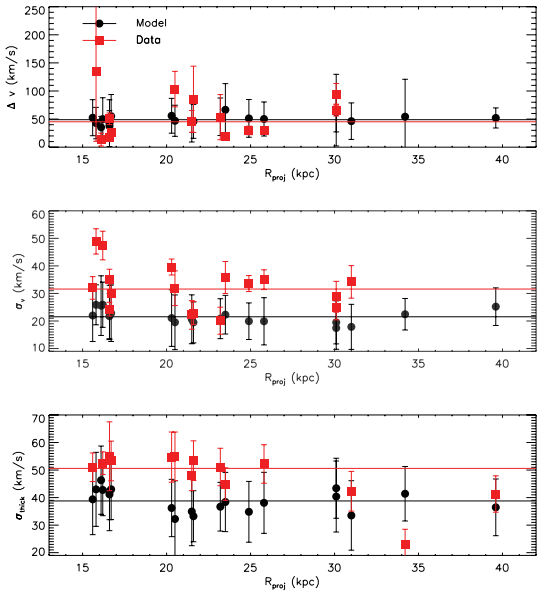

Figure 16. This figure compares the results from our data with results from our model analysed in the same way. In all cases, data are represented by filled red squares and dot–dashed lines, and the model results are shown as filled black circles and solid lines. Top panel: the difference in velocity, Δv, between the thin-disc and thick-disc components of data and model as a function of the projected radius. The model lag is consistent with no evolution with radius and shows an average lag of 48.9 km s^{-1}, very close to our input lag of 50 km s^{-1}. Middle panel: dispersion, $\sigma_{\rm thin}$, of the thin disc is plotted for both data and model as a function of the projected radius. The model thin disc is best fitted with an average dispersion of 21.5 km s^{-1}, very close to the input of 25.0 km s^{-1}. Lower panel: results for both the data and the model for the dispersion of the thick disc ($\sigma_{\rm thick}$) as a function of radius. For our model, the thick disc is consistent with no evolution with radius, unlike our data, and has an average dispersion of $\sigma_{\rm v} = 38.8$ km s^{-1}, which recovers our input dispersion of 40 km s^{-1} relatively well.

are quite different in terms of their mass from both the MW and M31, our values may be an overestimate. The M31 discs are also seemingly hotter than the MW discs, with $\sigma_{\rm thin,M31} = 32.0$ km s^{-1} (cf. $\sigma_{\rm thin,MW} = 20.0$ km s^{-1}) (Ivezić et al. 2008) and $\sigma_{\rm thick,M31} = 45.7$ km s^{-1} (cf. $\sigma_{\rm thick,MW} = 40.0$ km s^{-1}) (Ivezić et al. 2008). This could tell us something about the merger history of M31. If the thick discs in both galaxies are formed as a result of heating by mergers, the hotter discs of M31 could imply that this galaxy has undergone a more active merger history than the MW.

The MW thick disc is more metal poor, enriched in α metals and older than the thin disc. While we are unable to measure the age and α abundances of the M31 discs, we have shown that there exists an offset in the average metallicities of the two components of ∼0.2 dex when measured spectroscopically. While we do not see this offset photometrically, this could be due to our analysis technique as we use isochrones of the same α abundance ([α/Fe] = +0.2) and age (8 Gyr) for both components. If we modify the α-abundance and age of these isochrones to [α/Fe] = +0.4 and 10 Gyr for our thick-disc sample, respectively, we see an offset of ∼0.2 dex. We also note that both the thin and thick discs in M31 appear to be more metal poor than the MW discs, which have average metallicities of [Fe/H] ∼ −0.3 and ∼ −0.6 (Gilmore, Wyse & Norris 2002; Abadi et al. 2003; Carollo et al. 2010), respectively, although there is a significant metallicity spread in both discs. Carollo et al. (2010) also demonstrated evidence of a secondary, more metal poor thick disc in the MW, whose metallicities span the range $-1.8 \leq$ [Fe/H] $\leq$ −0.8, peaking at [Fe/H] = −1.3. This component also appears to be hotter than the traditional MW thick-disc component, with $\sigma_z = 44 \pm 3$ km s^{-1}, very similar to what we observe in M31.

Table 6. Average densities for the thin and thick discs in model fields from 100 MC realizations.

Field	$\rho_{*\rm thin}$ (N_*/arcmin^2)	$\rho_{*\rm thick}$ (N_*/arcmin^2)
228Mod	73.0 ± 35.2	31.0 ± 19.2
227Mod	15.7 ± 7.1	18.4 ± 8.1
166Mod	14.2 ± 7.7	14.1 ± 7.7
106Mod	11.9 ± 5.7	11.8 ± 5.7
105Mod	13.5 ± 6.3	10.8 ± 5.3
224Mod	10.6 ± 5.0	10.1 ± 4.8
232Mod	10.9 ± 6.1	7.6 ± 4.5
104Mod	10.7 ± 4.9	7.9 ± 3.8
220Mod	4.7 ± 1.8	4.2 ± 1.6
213Mod	4.6 ± 2.6	4.4 ± 2.4
102Mod	3.7 ± 1.5	3.8 ± 1.5
231Mod	3.8 ± 1.9	2.8 ± 1.3
223Mod	2.7 ± 1.0	2.7 ± 0.9
101Mod	2.9 ± 1.1	2.8 ± 1.0
222Mod	2.1 ± 0.7	2.1 ± 0.6
221Mod	1.7 ± 0.5	1.9 ± 0.5
50Mod	1.3 ± 0.3	1.2 ± 0.2
107Mod	1.4 ± 0.3	1.5 ± 0.3
w11Mod	1.4 ± 0.4	1.5 ± 0.3
167Mod	0.7 ± 0.4	0.5 ± 0.4
148Mod	0.6 ± 0.4	0.5 ± 0.3

In Section 4.1.3, we inferred scaleheights for the thin and thick discs of M31 of $h_z = 1.1 \pm 0.2$ and 2.8 ± 0.6 kpc, respectively, using a sample of 34 galaxies with thick discs measured by YD06 to determine a relationship between the scalelength and scaleheight of a stellar disc. As we noted in Section 4.1.3, a comparison with the YD06 sample might not be desirable, as these galaxies are typically much less massive than M31 and selected to be bulgeless. A more appropriate comparison would be the MW analogue, NGC 891, an edge-on galaxy that was recently the subject of a structural analysis by Ibata, Mouhcine & Rejkuba (2009) using *HST*/ACS imaging. They detected the presence of a thick-disc component in the galaxy and were able to measure both the scalelength and scaleheight for this component of $h_{\rm r} = 4.8 \pm 0.1$ kpc and $z_0 = 1.44 \pm 0.03$ kpc, compared with $h_{\rm r} = 4.2 \pm 0.01$ kpc and $z_0 = 0.57 \pm 0.01$ kpc for the thin-disc component in this galaxy. This gives a ratio of ∼1.1 between the scalelengths and ∼2.5 between the scaleheights of these components, which are identical to what we observe in M31. To illustrate this, we overplot these values for NGC 891 in Fig. 9 as a green circle.

In Yoachim & Dalcanton (2008b), the authors present kinematics of the thin and thick discs of nine of their initial sample of 34 galaxies, obtained using the GMOS on Gemini. To measure velocities and dispersions in both thin- and thick-disc components, they placed slits in positions corresponding to the mid-plane of the galaxy to measure the thin-disc properties and above the mid-plane where the contribution from the thin disc was thought to be negligible. As their typical velocity resolution was 60 km s^{-1}, they were unable to draw robust conclusions on the velocity dispersions of these components, but they were able to measure velocity rotation curves for each component and found a wide variety of behaviour amongst their thick-disc components, with discs which lagged behind the thin disc by only ∼5 km s^{-1}, discs that show no evidence of rotation and one case where the thick disc is counter-rotating

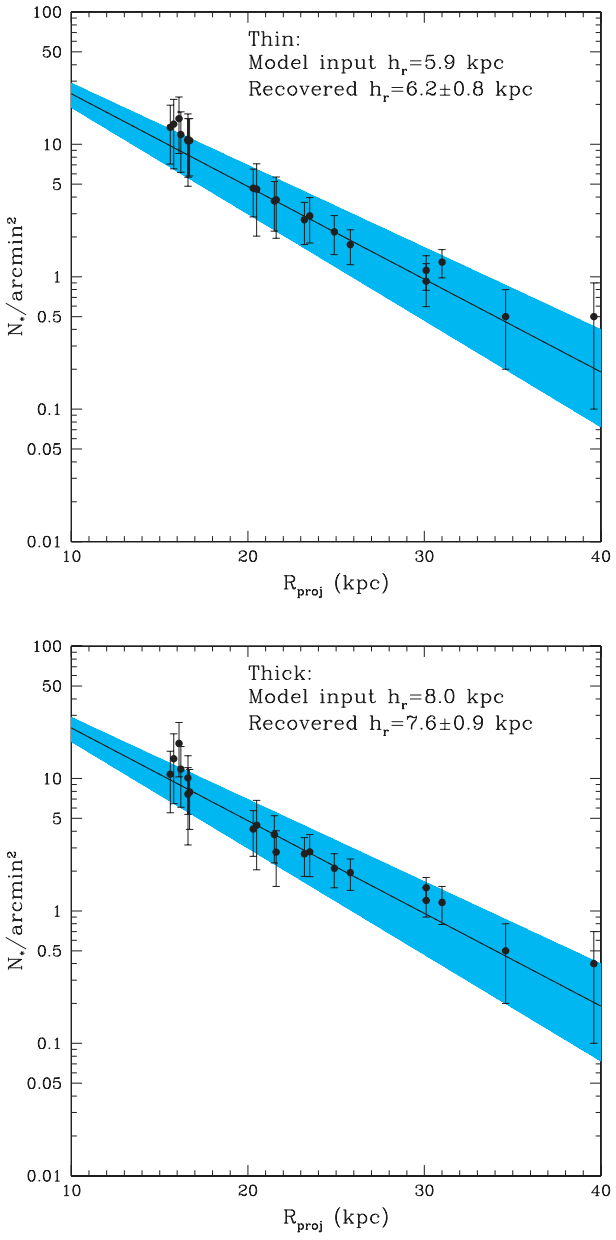

Figure 17. Results from MC recovery of the scalelengths in our thin- plus thick-disc model for our input thin (top panel) and thick (bottom panel) discs. The error bars on individual points represent the dispersion of calculated densities in the MC analysis, while the shaded regions represent the 1σ uncertainties from the weighted-least-squares fit. We recover a scalelength for the thin disc of $h_r = 6.2 \pm 0.8$ kpc and $h_r = 7.8 \pm 0.9$ for the thick disc, which are consistent with our input values.

with respect to the thin disc. The average lag between the thin- and thick-disc components of $\Delta v = 46.0\,\mathrm{km\,s^{-1}}$ we see in the M31 system is larger than the majority that they observe. We note that the galaxies in their sample were typically of much lower mass than M31 ($V_{\rm circ} < 150\,\mathrm{km\,s^{-1}}$ compared with $V_{\rm circ} \sim 230\,\mathrm{km\,s^{-1}}$). In the most massive of their sample (which are still less massive than M31), they do not detect a lag in the thick-disc kinematics at all and they attribute this to contrast issues. Their sample were also selected to be 'bulgeless', unlike M31 which has a significant bulge, and so a direct comparison may not be advisable. Owing to the wide range of kinematic behaviour exhibited in their sample, they conclude that the dominant formation process of thick discs is via minor mergers and accretions of satellites. In Yoachim & Dalcanton (2008a), they use Lick indices to measure ages and metallicities in nine low-mass galaxies with thick-disc components. While we measure an offset of 0.2 dex in the metallicities of the M31 thick and thin discs, they were unable to measure any such offset in their sample, though this could be a result of the insensitivity of Lick indices to such differences at low metallicity. They do find that the thick discs are host to older stellar populations than do the thin discs; however, with our current data set, we are unable to comment on the ages of stars in the M31 discs.

5.3 Possible formation scenarios

In this section, we discuss the various formation scenarios mentioned in Section 1. Owing to our inability to measure ages and vertical dispersions in M31, we are not able to confirm or reject any of these formation mechanisms at present, so we discuss additional constraints for these models that could help to rule out or confirm each scenario with further data and analysis.

5.3.1 Heating by minor mergers

Numerous studies have identified that impacts and mergers of satellites with masses less than a third of their hosts can kinematically heat the thin stellar disc, puffing it out into a substantially thicker disc (e.g. Quinn et al. 1993; Robin et al. 1996; Walker et al. 1996; Velazquez & White 1999; Chen et al. 2001; Sales et al. 2009; Villalobos & Helmi 2009). M31 is known to have recently undergone at least one significant minor-merger event, resulting in the GSS tidal stream. In recent work by Purcell et al. (2010), the authors model the heating of the stellar discs by minor mergers and trace disc stars ejected into the stellar halo by these simulated events. In addition to the stars ejected into the halo, they observe a concomitant increase in the number of stars located in the kinematic regime of the thick disc, contributing ∼10–20 per cent of the total stellar density along the major-axis, similar to what we observe in M31. They also find that their simulated planar infall produces two-component systems with scaleheights ($z_{\rm thin} \sim 1$ and $z_{\rm thick} \sim 3$ kpc), consistent with our measurements for M31. The similarities between our findings and those of Purcell et al. (2010) could suggest that thin-disc stars heated by the merging event that created the GSS may contribute some non-trivial fraction of stars to the thick disc.

According to the simulations of Kazantzidis et al. (2009), thick discs produced in this vein imprint a number of dynamical signatures on both the kinematic and the structural properties of the galaxy. These include considerable thickening and heating at all radii, prominent flaring, particularly in the outskirts of the disc (beyond 3 scalelengths), surface density excesses at large radii, radial anisotropies and substantial tilting of the disc. As M31 is not edge on, we are unable to comment on the evolution of the scaleheight of the thick disc with radius and so we cannot use this as a measure of flaring in the outer regions of the disc. However, one might expect that if there was a substantial flaring beyond 3 disc scalelengths (∼24 kpc), then this may be reflected by an increase in the velocity dispersions of both thin- and thick-disc components. Our results for evolution in the thin- and thick-disc dispersions remain inconclusive, and so it is possible that such flaring may exist. At present, we possess few fields between $R \sim 32$ and 39.6 kpc, so populating this region with kinematics, as well as additional fields farther out, may further enlighten us to any potential flaring. Another test of this formation scenario would be to include fields from

both the minor-axis and the NE portion of M31 to test for any radial anisotropy, assuming one can reliably disentangle contamination from foreground and substructure from the signatures of the discs. The work of Sales et al. (2009) also tells us that thick discs that are produced as a result of heating present structures with low orbital eccentricity.

5.3.2 Accretion of a satellite on a coplanar orbit

Numerical simulations by Abadi et al. (2003) and Peñarrubia, McConnachie & Babul (2006) show that an old, thick disc of stars could form via the accretion of stars from satellite galaxies on an approximately coplanar orbit with its host. Such discs are similar in radial extent and contain older stellar populations when compared with the thin disc. The thick disc we find in M31 is consistent with this model in so far as the radial extents of both discs (5.9–7.3 and 8.0 kpc) are comparable with one another. They also argue that the mass and luminosity of the progenitor satellite can be inferred from the metallicity of the component. We deduce $[\mathrm{Fe/H}]_{\mathrm{thick}} = -1.0 \pm 0.1$ for M31, which would correspond to a satellite of $M_V \sim -15$ ($L_{\mathrm{v}} \sim 9 \times 10^7\,\mathrm{L}_{\odot}$), similar to the M31 dwarf elliptical NGC 147 ($M_V = -15.1$, van den Bergh 1999). However, given the mass we calculate for the thick disc in Section 4.1.4 of (2–4) $\times\ 10^{10}\,\mathrm{M}_{\odot}$, it seems very unlikely that the thick disc of M31 could have been formed from such a satellite.

Results of the simulations of Sales et al. (2009) show that stars accreted into a thick disc from satellites on coplanar orbits exhibit high-eccentricity orbits. Our present data set does not allow us to probe the eccentricity of the orbits within the thick disc at this time. With a larger data set, we could perhaps see the effects of orbital differences in the form of structural asymmetries.

5.3.3 Radial migration and internal heating

The scattering of stars by spiral structure and molecular clouds has long been proposed as a method of heating the stellar disc, moving stars out on to more eccentric and inclined orbits (Sellwood & Binney 2002; Haywood 2008; Roškar et al. 2008; Schönrich & Binney 2009a), and it has been argued in Schönrich & Binney (2009a,b) that these processes naturally produce an old, α-enhanced thick disc, whose properties are consistent with those observed in the MW. These models also show wide MDFs and an increase in the scatter of the age–metallicity relation. This is also demonstrated in Quillen et al. (2009), where they investigate radial mixing induced by an orbiting subhalo. Again they find evidence of wide MDFs in both the thin and the thick discs. With deeper photometry that allowed us to reach the MSTOs of the two discs, we could derive the average ages of these components, and with high-resolution spectroscopy ($R \sim 15\,000$) of M31 thick-disc stars that would allow us to determine accurate abundances from unblended Fe lines for individual stars, we could comment more robustly on the likelihood of such a formation scenario.

5.3.4 Thick disc forms thick

Kroupa (2002) posited that thick discs could be formed as a result of vigorous star formation in massive star clusters ($\sim 10^5$–$10^6\,\mathrm{M}_{\odot}$) during the period of assembly of the stellar disc. If this is true, a number of these massive clusters may have survived to the present day and would possess large vertical velocity dispersions. Kroupa (2002) suggests that these clusters could be the metal-rich globular cluster system in the MW. Once again, owing to the inclination of M31, we are unable to measure the vertical dispersions of its metal-rich globular cluster system and can therefore neither confirm nor reject this formation model.

6 CONCLUSIONS

Using the DEIMOS on the Keck II telescope, we have identified a statistically significant population of stars in M31 that lags behind the thin and extended discs by $46.0 \pm 3.9\,\mathrm{km\,s^{-1}}$. Comparing this with a model of a thin- plus thick-disc system with the same distance and inclination as M31 shows this component to be consistent with a thick-disc component. Analysing its kinematics, we find it to be hotter than the thin disc, with an average dispersion $\sigma_{\mathrm{thick}} = 50.8 \pm 1.9\,\mathrm{km\,s^{-1}}$ (cf. $\sigma_{\mathrm{thin}} = 35.7 \pm 1.0\,\mathrm{km\,s^{-1}}$) larger than the dispersions observed in the MW discs. From composite spectra for each component, constructed from highly probable thin- and thick-disc stars (selected using stringent Gaussian cuts), we measure a metallicity offset of $\sim$0.3 dex between the two discs, with the thick disc being more metal poor than the thin disc ($[\mathrm{Fe/H}]_{\mathrm{thick}} = -1.0 \pm 0.1$ compared with $[\mathrm{Fe/H}]_{\mathrm{thin}} = -0.7 \pm 0.05$). The fact that this metallicity offset is not observed when analysing the thin- and thick-disc RGB stars with isochrones of identical age and α-abundance suggests that the two populations differ in these properties, with the thick disc likely being older and more enriched in α elements.

We measure scalelengths for both the thin and the thick discs, finding $h_{\mathrm{r}} = 8.0 \pm 1.2$ kpc for the thick disc and $h_{\mathrm{r}} = 7.3 \pm 1.1$ kpc for the thin disc, comparable to previous estimates. Using the data of YD06, we infer scaleheights at $z_0 = 2.8 \pm 0.6$ and 1.1 ± 0.2 kpc for the thick and thin discs, respectively. These values are of the order of two to three times larger than those measured in the MW, perhaps suggesting that M31 has undergone more heating than our Galaxy.

By measuring the ratio of the densities of both discs, we are able to estimate a mass range for the thick-disc component of $2.4 \times 10^{10} < M_{*,\mathrm{thick}} < 4.1 \times 10^{10}\,\mathrm{M}_{\odot}$. This value provides a useful constraint on possible formation mechanisms, as any proposed method for forming a thick disc must be able to heat (or deposit) at least this amount of material.

Owing to current limitations within our data set, we are not able to distinguish between the different thick-disc formation mechanisms. However, with further analysis of this component using our complete kinematic sample (including regions from the minor-axis and NE of M31) and spectroscopic follow-up of fields where this component is strongly observed, we will be able to better understand the chemistry of this component and distinguish between various formation mechanisms.

ACKNOWLEDGMENTS

MLMC would like to acknowledge the support of an STFC studentship. GFL acknowledges the award of the Cambridge Raymond & Beverly Sackler distinguished visitor fellowship.

REFERENCES

Abadi M. G., Navarro J. F., Steinmetz M., Eke V. R., 2003, ApJ, 597, 21
Alves-Brito A., Meléndez J., Asplund M., Ramírez I., Yong D., 2010, A&A, 513, A35
Ashman K. M., Bird C. M., Zepf S. E., 1994, AJ, 108, 2348
Battaglia G., Irwin M., Tolstoy E., Hill V., Helmi A., Letarte B., Jablonka P., 2008, MNRAS, 383, 183

Bensby T., Alves-Brito A., Oey M. S., Yong D., Meléndez J., 2010, A&A, 516, L13
Benson A. J., Lacey C. G., Frenk C. S., Baugh C. M., Cole S., 2004, MNRAS, 351, 1215
Bournaud F., Elmegreen B. G., Martig M., 2009, ApJ, 707, L1
Braun R., Thilker D. A., Walterbos R. A. M., Corbelli E., 2009, ApJ, 695, 937
Brinks E., Burton W. B., 1984, A&A, 141, 195
Brook C. B., Kawata D., Gibson B. K., Freeman K. C., 2004, ApJ, 612, 894
Brook C., Richard S., Kawata D., Martel H., Gibson B. K., 2007, ApJ, 658, 60
Brooks A. M., Governato F., Quinn T., Brook C. B., Wadsley J., 2009, ApJ, 694, 396
Brown T. M., Smith E., Ferguson H. C., Rich R. M., Guhathakurta P., Renzini A., Sweigart A. V., Kimble R. A., 2006, ApJ, 652, 323
Burstein D., 1979, ApJ, 234, 829
Carlberg R. G., 1987, ApJ, 322, 59
Carollo D. et al., 2010, ApJ, 712, 692
Cash W., 1979, ApJ, 228, 939
Chapman S. C., Ibata R., Lewis G. F., Ferguson A. M. N., Irwin M., McConnachie A., Tanvir N., 2005, ApJ, 632, L87
Chapman S. C., Ibata R., Lewis G. F., Ferguson A. M. N., Irwin M., McConnachie A., Tanvir N., 2006, ApJ, 653, 255
Chapman S. C. et al., 2007, ApJ, 662, L79
Chapman S. C. et al., 2008, MNRAS, 390, 1437
Chemin L., Carignan C., Foster T., 2009, ApJ, 705, 1395
Chen B. et al., 2001, ApJ, 553, 184
Chen Y. Q., Zhao G., Zhao J. K., 2009, ApJ, 702, 1336
Chiba M., Beers T. C., 2000, AJ, 119, 2843
Choi P. I., Guhathakurta P., Johnston K. V., 2002, AJ, 124, 310
Choi Y., Park C., Vogeley M. S., 2007, ApJ, 658, 884
Collins M. L. M. et al., 2009, MNRAS, 396, 1619
Collins M. L. M. et al., 2010, MNRAS, 407, 2411
Corbelli E., Lorenzoni S., Walterbos R., Braun R., Thilker D., 2010, A&A, 511, A89
Dalcanton J. J., Bernstein R. A., 2002, AJ, 124, 1328
de Jong J. T. A., Yanny B., Rix H., Dolphin A. E., Martin N. F., Beers T. C., 2010, ApJ, 714, 663
Delgado Serrano R., Hammer F., Yang Y. B., Puech M., Flores H., Rodrigues M., 2010, A&A, 509, A78
Dotter A., Chaboyer B., Jevremovic D., Kostov V., Baron E., Ferguson J. W., 2008, ApJS, 178, 89
Dubinski J., Gauthier J., Widrow L., Nickerson S., 2008, in Funes J. G., Corsini E. M., eds, ASP Conf. Ser. Vol. 396, Spiral and Bar Instabilities Provoked by Dark Matter Satellites. Astron. Soc. Pac., San Francisco, p. 321
Elmegreen B. G., Elmegreen D. M., 2006, ApJ, 650, 644
Ferguson A. M. N., Johnson R. A., 2001, ApJ, 559, L13
Ferguson A. M. N., Irwin M. J., Ibata R. A., Lewis G. F., Tanvir N. R., 2002, AJ, 124, 1452
Geehan J. J., Fardal M. A., Babul A., Guhathakurta P., 2006, MNRAS, 366, 996
Geha M., Guhathakurta P., Rich R. M., Cooper M. C., 2006, AJ, 131, 332
Gilbert K. M. et al., 2006, ApJ, 652, 1188
Gilbert K. M. et al., 2009, ApJ, 705, 1275
Gilmore G., Reid N., 1983, MNRAS, 202, 1025
Gilmore G., Wyse R. F. G., Norris J. E., 2002, ApJ, 574, L39
Hammer F., Flores H., Elbaz D., Zheng X. Z., Liang Y. C., Cesarsky C., 2005, A&A, 430, 115
Hammer F., Puech M., Chemin L., Flores H., Lehnert M. D., 2007, ApJ, 662, 322
Hänninen J., Flynn C., 2002, MNRAS, 337, 731
Hayashi H., Chiba M., 2006, PASJ, 58, 835
Haywood M., 2008, MNRAS, 388, 1175
Holland S., Fahlman G. G., Richer H. B., 1996, AJ, 112, 1035
Hopkins P. F., Hernquist L., Cox T. J., Younger J. D., Besla G., 2008, ApJ, 688, 757
Hopkins P. F., Cox T. J., Younger J. D., Hernquist L., 2009, ApJ, 691, 1168
Howley K. M., Geha M., Guhathakurta P., Montgomery R. M., Laughlin G., Johnston K. V., 2008, ApJ, 683, 722
Ibata R., Irwin M., Lewis G., Ferguson A. M. N., Tanvir N., 2001, Nat, 412, 49
Ibata R., Chapman S., Ferguson A. M. N., Lewis G., Irwin M., Tanvir N., 2005, ApJ, 634, 287 (I05)
Ibata R., Martin N. F., Irwin M., Chapman S., Ferguson A. M. N., Lewis G. F., McConnachie A. W., 2007, ApJ, 671, 1591
Ibata R., Mouhcine M., Rejkuba M., 2009, MNRAS, 395, 126
Irwin M. J., Ferguson A. M. N., Ibata R. A., Lewis G. F., Tanvir N. R., 2005, ApJ, 628, L105
Ivezić Ž. et al., 2008, ApJ, 684, 287
Jurić M. et al., 2008, ApJ, 673, 864
Just A., Jahreiß H., 2010, MNRAS, 402, 461
Kalirai J. S. et al., 2006, ApJ, 648, 389
Kalirai J. S. et al., 2010, ApJ, 711, 671
Kazantzidis S., Zentner A. R., Kravtsov A. V., 2006, ApJ, 641, 647
Kazantzidis S., Zentner A. R., Kravtsov A. V., Bullock J. S., Debattista V. P., 2009, ApJ, 700, 1896
Klypin A., Zhao H., Somerville R. S., 2002, ApJ, 573, 597
Koch A. et al., 2008, ApJ, 689, 958
Kormendy J., Bender R., 1999, ApJ, 522, 772
Kroupa P., 2002, MNRAS, 330, 707
Loebman S. R., Roskar R., Debattista V. P., Ivezic Z., Quinn T. R., Wadsley J., 2010, preprint (ArXiv e-prints)
McConnachie A. W., Irwin M. J., Lewis G. F., Ibata R. A., Chapman S. C., Ferguson A. M. N., Tanvir N. R., 2004a, MNRAS, 351, L94
McConnachie A. W., Irwin M. J., Ferguson A. M. N., Ibata R. A., Lewis G. F., Tanvir N., 2004b, MNRAS, 350, 243
McConnachie A. W., Irwin M. J., Ferguson A. M. N., Ibata R. A., Lewis G. F., Tanvir N., 2005, MNRAS, 356, 979
McConnachie A. W. et al., 2009, Nat, 461, 66
Meléndez J. et al., 2008, A&A, 484, L21
Merrett H. R. et al., 2006, MNRAS, 369, 120
Park C., Choi Y., Vogeley M. S., Gott J. R., III, Blanton M. R., 2007, ApJ, 658, 898
Peñarrubia J., McConnachie A., Babul A., 2006, ApJ, 650, L33
Pohlen M., Dettmar R., Lütticke R., 2000, A&A, 357, L1
Purcell C. W., Kazantzidis S., Bullock J. S., 2009, ApJ, 694, L98
Purcell C. W., Bullock J. S., Kazantzidis S., 2010, MNRAS, 404, 1711
Quillen A. C., Minchev I., Bland-Hawthorn J., Haywood M., 2009, MNRAS, 397, 1599
Quinn P. J., Hernquist L., Fullagar D. P., 1993, ApJ, 403, 74
Read J. I., Lake G., Agertz O., Debattista V. P., 2008, MNRAS, 389, 1041
Reddy B. E., Lambert D. L., Allende Prieto C., 2006, MNRAS, 367, 1329
Richardson J. C. et al., 2008, AJ, 135, 1998
Robertson B., Bullock J. S., Cox T. J., Di Matteo T., Hernquist L., Springel V., Yoshida N., 2006, ApJ, 645, 986
Robin A. C., Haywood M., Creze M., Ojha D. K., Bienayme O., 1996, A&A, 305, 125
Robin A. C., Reylé C., Derrière S., Picaud S., 2004, A&A, 416, 157
Roškar R., Debattista V. P., Quinn T. R., Stinson G. S., Wadsley J., 2008, ApJ, 684, L79
Roškar R., Debattista V. P., Brooks A. M., Quinn T. R., Brook C. B., Governato F., Dalcanton J. J., Wadsley J., 2010, MNRAS, 408, 783
Rutledge G. A., Hesser J. E., Stetson P. B., 1997, PASP, 109, 907
Saglia R. P. et al., 2010, A&A, 509, A61
Sales L. V. et al., 2009, MNRAS, 400, L61
Schönrich R., Binney J., 2009a, MNRAS, 396, 203
Schönrich R., Binney J., 2009b, MNRAS, 399, 1145
Seigar M. S., Barth A. J., Bullock J. S., 2008, MNRAS, 389, 1911
Sellwood J. A., Binney J. J., 2002, MNRAS, 336, 785
Sellwood J. A., Nelson R. W., Tremaine S., 1998, ApJ, 506, 590
Shaw M. A., Gilmore G., 1989, MNRAS, 237, 903
Simon J. D., Geha M., 2007, ApJ, 670, 313
Soubiran C., Bienaymé O., Siebert A., 2003, A&A, 398, 141
Stewart K. R., Bullock J. S., Wechsler R. H., Maller A. H., Zentner A. R., 2008, ApJ, 683, 597

Stewart K. R., Bullock J. S., Barton E. J., Wechsler R. H., 2009, ApJ, 702, 1005
Toth G., Ostriker J. P., 1992, ApJ, 389, 5
Tsikoudi V., 1979, ApJ, 234, 842
van den Bergh S., 1999, A&AR, 9, 273
van der Kruit P. C., 1984, A&A, 140, 470
van der Kruit P. C., Searle L., 1981, A&A, 95, 105
van Dokkum P. G., Peletier R. F., de Grijs R., Balcells M., 1994, A&A, 286, 415
Velazquez H., White S. D. M., 1999, MNRAS, 304, 254
Villalobos Á, Helmi A., 2009, MNRAS, 399, 166
Villumsen J. V., 1985, ApJ, 290, 75
Walker I. R., Mihos J. C., Hernquist L., 1996, ApJ, 460, 121
Walterbos R. A. M., Braun R., 1994, ApJ, 431, 156
Walterbos R. A. M., Kennicutt R. C., Jr, 1988, A&A, 198, 61
Widrow L. M., Perrett K. M., Suyu S. H., 2003, ApJ, 588, 311
Wyse R. F. G., Gilmore G., Norris J. E., Wilkinson M. I., Kleyna J. T., Koch A., Evans N. W., Grebel E. K., 2006, ApJ, 639, L13
Yin J., Hou J. L., Prantzos N., Boissier S., Chang R. X., Shen S. Y., Zhang B., 2009, A&A, 505, 497
Yoachim P., Dalcanton J. J., 2006, AJ, 131, 226 (YD06)
Yoachim P., Dalcanton J. J., 2008a, ApJ, 683, 707
Yoachim P., Dalcanton J. J., 2008b, ApJ, 682, 1004

This paper has been typeset from a TEX/LATEX file prepared by the author.